Geometry and growth of syn-tectonic plutons emplaced in thrust shear zones: Insights from Abu Ziran Pluton, Egypt

Abdullah T. Mohammad[a, b]* and Y. A. El Kazzaz[b]

[a]*Department of geological and environmental sciences, Western Michigan University, Kalamazoo, Michigan, USA*

[b]*Department of geology, Helwan University, Cairo, Egypt*

Email for the *corresponding author: Ibrahim.Abdullahtarekmohammad@wmich.edu

Authors' details

Abdullah T. Mohammad; Ibrahim.Abdullahtarekmohammad@wmich.edu,

Yahia A. El Kazzaz; yahia.elkazzaz@science.helwan.edu.eg

This paper was submitted to Journal of structural geology (https://www.sciencedirect-.com/journal/journal-of-structural-geology)

Abstract

Coupling of deformation and magmatism has been reported in several old orogenic belts, particularly along thrust faults and shear zones. The syn-kinematic plutons in exhumed shear zones offer the best opportunity to understand the complex relationship between magmatism and regional deformation. The present paper investigates the geometry and internal structure of granite plutons emplaced in thrust faults and shear zones, and structural control on their emplacement mechanism. Abu Ziran pluton is an example of the intrusions emplaced in active brittle-ductile zones in the Nubian shield, and documents clear evidence on the interaction between magmatism and regional deformation during melt ascent and emplacement. Results from detailed geological mapping, remote sensing, and structural analysis of the pluton and associated highly strained rocks permitted the constraining of the pluton's geometry, emplacement mechanism, and spatio-temporal evolution. Structural analysis of the study area indicates that pluton emplacement was syn- to-late-tectonic. The brittle-ductile fabrics in the wall rock are consistent with a sub-horizontal thrust shear zone with a top-to-NW shear sense. The activity of the shear zone was accompanied by an episode of a calc-alkaline magmatic pulse. Granitic magma ascended upward via non-exposed feeder dykes, or through ramps and flats in the thrust system and emplaced laterally along the shear zone, forming complex sub-horizontal sheet-shaped intrusion. The geometry and extent of pluton emphasize that inherited heterogeneities and regional stress states played important role in the emplacement processes. In addition, localization of pluton along or near the contact between ophiolitic nappes and mylonitic metasediments suggests that the rheological boundaries act as barriers that impedes the rise of ascending magma, causing magma arrest, and triggers lateral spreading and emplacement. The outcomes of this study allowed the reconstruction of the geometry and internal structure of Abu Ziran pluton and an understanding of its evolution in space and time.

1. Introduction

The coupling of deformation and magmatism received the attention of the structural geology community since the seventies of the last century, yet an exhaustive grasping for the nature of the spatial and temporal relationships between two processes remains elusive (e.g., Pitcher, 1979; Pitcher and Bussell, 1977; Hutton, 1982, 1988; Wadge and Cross, 1988; Hutton and Reavy, 1992; Vigneresse, 1995; Brown et al., 1997; Roman-Berdiel et al., 1997; Brown and Solar, 1998; Musumeci et al., 2005; Žák et al., 2013). Evidences of the pairing of plutons and shear zones have been widely reported in different the tectonic settings including extensional (e.g., Hutton, 1988), transcurrent (e.g., Hutton, 1982; McCaffrey, 1992; Neves et al., 1996;

Weinberg et al., 2004) and compressional regimes (e.g., Davidson et al., 1992; D’Lemos et al., 1992; Musumeci et al., 2005; Ferre´ et al., 2012). The accumulated data provoked a growing perception that a causative link exists between the two processes, either shear zones control the ascent and emplacement of magma at different crustal levels (Brown and Solar, 1998; Petford and Koenders, 1998; Weinberg et al., 2004, 2005), or the magma emplacement affects the rheology of host rocks and triggers strain localization and nucleation of shear zones on pluton margins (e.g., Neves and Vauchez, 1995; Neves et al., 1996; Neves and Mariano, 1999; Vigneresse and Tikoff 1999; Vigneresse et al., 1999; Cao and Neubauer, 2016). Rosenberg (2004) compiled data from Alpine granite plutons, and concluded that, with few exceptions, there is a clear spatial and temporal relationship between shear zones and emplacement and distribution of plutons. In contrast to this thought, some authors used statistical analyses of spatial and geometrical data from several plutons and volcanic features to refute any coupling between magma ascent and emplacement, and shear zones activity (e.g., Paterson and Schmidt, 1999; Schmidt and Paterson, 2000; Paterson, 2005).

The remark of deformation and magmatism link has coincided with an expanding interest in understanding the geometry of syn-kinematic plutons and structural control of their shapes (e.g., Davies 1982; De Wit et al., 1987; McCaffrey 1989, 1992; Hutton 1996; Nyman and Karlstrom 1997; Petford et al., 2000; Ferguson et al., 2004; Musumeci et al., 2005; Ferre´ et al., 2012). Contrary to the classic diapiric model, which pictured intrusions as vertical-sided bodies with deep roots in the crust, the overwhelming results from field studies, geophysical investigation, deformation experiments, and numerical modeling clearly emphasized that syn-kinematic plutons tend to grow as tabular or sheet-shaped intrusions of different orders of magnitudes, and are fed by one or more feeder dykes (e.g., Myers1975; Pitcher 1979; Hutton 1982, 1996; Hutton et al.,1990; Ingram and Hutton 1994; Vigneresse 1995; Weinberg et al., 2004; Köpping et al., 2022). These tabular intrusions do not necessarily propagate as a simple continuous sheet but may initiate as closely spaced small sheets that inflate and coalesce into complex sheet intrusion (e.g., Schofield et al., 2012; Magee et al., 2016; Galland et al., 2019; Köpping et al., 2022). Also, they can be built by one or series of incremental magmatic pulses, which take over thousands to millions of years (Michel et al., 2008; Horsman et al., 2009). The geometry of sheet intrusions is principally controlled by the stress state during emplacement, as plutons tend to be oriented orthogonal to $\sigma3$ and parallel to the $\sigma1$- $\sigma2$ plane (Anderson, 1951; Gautneb and Gudmundsson, 1992; Muirhead et al., 2015, Magee et al., 2019). However, Hutton (1992) underlined that geometry and weaknesses of the shear zones also plays a significant role in the final geometry of the pluton.

Despite the extensive work, the bulk of research has been devoted to plutons in extensional and transcurrent regimes, and only a few papers shed light on the geometry of granite sheets emplaced along thrust faults (e.g., Karlstrom et al., 1993; Searle 1999; Ferré et al., 2002, 2012; Musumeci et al., 2005). Detailed knowledge regarding the geometry and emplacement mechanisms of plutons emplaced along thrust shear zones is still vague. Further, there is yet an ongoing debate about magma ascent and emplacement in regions of dominant compressional stresses which are considered to be sites of space denying conditions (e.g., Hamilton 1994; Hutton 1996; Watanabe et al., 1999). Several field-based studies have drawn attention to the close relationship between pluton emplacement and the geometry of flats and ramps in the active thrust faults (e.g., Shimura 1992; Karlstrom et al., 1993; Toyoshima et al., 1994; Searle 1999; Kalakay et al., 2001; Musumeci et al., 2005; Naibert et al., 2010). Hutton (1996) stressed the role of sites of local dilation along thrust faults as potential sites for accommodating ascending magma, especially in the middle and upper crustal levels. Furthermore, some authors discussed the role of the inherited, pre-existing weaknesses (faults and fractures) in inactive shear zones that act as preferable pathways for syn- and post-kinematic magma emplacement (e.g., Sibson 2003).

The Abu Ziran granite pluton, located in the Central Eastern Desert (CED) of Egypt, is a striking example of syn-tectonic plutons emplaced in compressional regime. The pluton intruded a sub-horizontal ductile shear zone commonly known as Eastern Desert Shear Zone (EDSZ; Andresen et al., 2010; Johnsen et al., 2011), Eastern Desert Décollement (EDD; Stern 2018), or Meatiq shear zone (MSZ; Mohammad et al., 2020) during late Neoproterozoic. The well-exposed floor and roof contacts and clearly documented relationships among the pluton and fabrics in country rocks, making it suitable for understanding the geometrical aspects of intrusions placed along active shear zones. Abu Ziran pluton has been the subject of several publications in the last three decades that attempt to explain the structural control on the emplacement of the granite intrusion (e.g., Fritz and Puhl 1996; Fritz et al., 1996, 2014). Nevertheless, less attention has been paid to reconstructing the 3D geometry of the pluton and understanding its spatio-temporal evolution. The present work combines multi-scale structural observations and data from field mapping, remote sensing, microstructural analysis, and relevant published data to unravel the 3D geometry, emplacement mechanism, and spatio-temporal evolution of Abu Ziran pluton. The results unveil significant insights regarding the geometry and emplacement mechanisms of the syn-kinematic plutons. In addition, the paper discusses the possible mechanisms of room creation required for accommodating pluton emplacement in compressional regimes.

2. Regional Geology

2.1 Geology of Central Eastern Desert

The CED province of Egypt (Figs.1a, b) is a significant structural segment of the Egyptian Nubian Shield which grew and evolved through a multicyclic history of magmatic, metamorphic, and deformation episodes during the Neoproterozoic (800- 600 Ma; Johnson et al., 2011; Zoheir et al., 2015; Stern 2018). It represents a distinct domain of accretion- and collision-related stacked thrust nappes associated with the Ediacaran assembly of Gondwanaland (Stern 1994), which were overprinted by arrays of subsequent ductile and brittle structures (e.g., Ries et al., 1983; Greiling et al., 1994; Fritz et al., 1996; Fowler and El Kalioubi 2004; Shalaby et al., 2005; Abd El Wahed 2008, 2010; Kiyokawa et al., 2020a, b; Zoheir et al., 2021).

2.1.1 Tectonostratigraphy and granite intrusions

The CED is thought to have a tiered architecture with two distinct structural levels (Bennett and Mosley, 1987; Greiling et al., 1994). The lower level (Tier-1 or infrastructure) consists of amphibolite facies schists, mylonites, and gneisses, while the upper one (Tier-2 or suprastructure) comprises a sheared ensimatic suit of ophiolitic rocks and mélange, island-arc metavolcanics, and molasse sediments (e.g., El Gaby et al., 1984, 1988; Stern 2018). Tier-1 exposures are limited to the cores of gneissic domal structures in the CED (Fig.1c) such as Meatiq (Sturchio et al., 1983; Habib et al., 1985a, b; Andresen et al., 2010); El Sibai (Kamal E1 Din 1992; Fritz et al., 2002; Breger et al., 2002), Um Had (Fowler and Osman 2001; Abu Sharib et al., 2019), and El Shalul (Ali et al., 2012). The contact between the two tiers is defined by a mylonitic carapace which is interpreted as a regional sub-horizontal shear zone, known as Eastern Desert Shear Zone (EDSZ; Andresen et al., 2010) or the Eastern Desert Décollement (EDD; Stern 2018). It is exposed in the domes as a folded zone of mylonites that detach the amphibolite facies rocks in the core from the upper allochthonous suit (Sturchio et al., 1983; Andresen et al., 2010). This sheared contact acts as a crustal-scale detachment surface that separates two distinct realms of different structural, metamorphic, and rheological attributes (Stern 2018). However, Fowler and Osman (2001) pointed out that there is no reason to suppose that all the two units are separated by a single continuous shear surface.

Both tectonostratigraphic units of the CED were imperiled to several pulses of magmatism, lasted from Tonian to Ediacaran Periods (800- 550 Ma) and manifested by a plethora of deformed and undeformed granite intrusions (Lundmark et al., 2012). The deformed granitic intrusions were referred to as “older granites” which interpreted as syn-orogenic plutons, while the undeformed intrusions were known as “younger granites” and are assumed to be late- to post-orogenic (Bentor, 1985; Johnson et al., 2011). This link between pronounced deformation in older granites and orogenic (compressional) processes was questioned by Fritz et al., (2014), as penetrative fabric may be also imposed by extensional tectonics.

2.1.2 Structural setting and history

The nappe pile of the CED was transected by several strands of NW-trending, kilometer-scale transcurrent sinistral shear zones, defined by anastomosing belts of highly foliated rocks that slice up the CED into discrete structural blocks with complex patterns (Fig.1b). These shear zones are accepted by most authors as northern extensions for the Najd Fault System (NFS) in the CED (e.g., Stern 1985; Sultan et al., 1988; Fritz et al., 1996, 2002; Shalaby et al., 2005). Even Though the accumulated wealth of structural data, there is still a lack of agreement regarding the tectonic and deformation history of the CED. Here we will follow the semi-consensual synthesized scheme of Johnson et al., (2011), and consider the identification of differences between models, if necessary.

The earliest phase, as all authors agree, was dominated by NW-SE shortening accompanying the accretion and suturing of the juvenile ensimatic assemblage. This episode was manifested in the CED by a system of stacked thrust nappes with a dominant NW-tectonic transport, collectively identified as “Pan-African nappe complex” that placed the low-grade supracrustal rocks over high-grade infracrustal gneisses and migmatites (e.g., Ries et al., 1983; Habib et al., 1985a, b; El Gaby et al. 1988, 1990; Fritz et al., 1996; Andresen et al., 2010). The timing of this phase is a matter of controversy, as Johnson et al, (2011) suggested it has lasted from 700 to 640 Ma, others bracketed the ceasing of this stage to about 606-600 Ma (Andresen et al., 2009). The subsequent stages are not agreed.

Johnson et al, (2011) followed Abdeen and Greiling (2005) in their inference of the presence of a period of gravitational collapse with NW–SE to NNW–SSE extension, probably occurred in the timespan between about 640 Ma and 630 Ma and resulted in the formation of Hammamat molasse basins. Similarly, a period of lithospheric extension due to gravitational sliding has been advocated by Fowler and El Kalioubi (2004) to interpret the origin of the top-to-NW tectonic transport in the CED, which manifested by the high-strain shear zones exposed in the contacts of gneissic domes, and formation of molasse basins. An alternative interpretation for this top-to-NW transport phase was introduced by Andresen et al., (2009) which attributed this tectonic transport to compressional rather than extensional phase. In their model, the molasse sediments were deemed as syn-orogenic sediments, accumulated in piggy-back foreland basins or strike-slip basins in front of a NW-propagating thrust front.

This phase was followed a period of transpression associated with a bulk E–W to ENE–WSW shortening, and manifested by NW-SE- trending folds, thrust faults with SW-directed transport, and NW-SE sinistral strike-slip faults (Fowler and Osman, 2001; Abdeen and Greiling, 2005; Andresen et al., 2010; Mohammad et al., 2020). After the ceasing of the orogenic pulses, the northern part of the Nubian shield was subjected to wide-spread regional N-S to NW-SE extension between about 600 Ma and 565 Ma, expressed in the NE- striking normal faults and dyke swarms (Stern 1985; Johnson et al., 2011).

Contrary to this scheme, there is another considerable and accepted model for interpreting the structural history of the CED, which links its evolution with the tectonic activity of the NFS (e.g., Fritz et al., 1996, 2002; Breger et al., 2002). In this envision, after the earlier accretion and stacking, CED were subjected to bulk E-W shortening which has been partitioned into domains of NW-trending strike-slip shear zones, and fold and fold-thrust belts with dominantly SW-directed transport (Fritz et al., 1996). The NFS strands define fault-bounded wrench corridors which accommodated the simultaneous orthogonal shortening and extension and have been considered by some workers the main governing structures for the exhumation of gneiss domes, and formation of molasse sedimentary basins (Fritz et al., 1996, 2002; Fritz and Messner 1999; Breger et al., 2002; Shalaby et al., 2006; Abd El-Wahed 2008; Shalaby 2010; Hamimi and Abd El-Wahed 2020).

2.2 Geology of Meatiq area

Meatiq dome is a map-scale, elliptical domal structure with a 22 km long and 18 km width. On satellite images, the domal structure is easily detected with the distinctive elliptical shape and well-marked outward dipping of structural units and foliation (Fig.1c). The western side of the Meatiq dome is truncated by the NW-SE trending, pervasive Atalla Shear Zone (ASZ), which comprises a major transpressional shear zone with a sinistral sense of shear (Mohammad et al. 2020). Fitz et al., (1996, 2002) demarcated the eastern and western borders of Meatiq dome by two NW-trending, strike-slip faults with sinistral sense. Foliation trajectories inside Meatiq dome define two major, NW-trending antiformal structures (Fig.): (1) Um Baanib antiform in the eastern side, and (2) Um Esh El-Hamra antiform in the western side. The two folds are separated by a major synformal structure known as Abu Ziran synform (Mohammad et al., 2020). Restoring the pre-doming geometry of the Meatiq shear zone reveals an original sub-horizontal ductile thrust zone (MSZ) with a top-to-NW sense of shearing (Mohammad et al., 2020). As a consequence of NE-SW shortening, the shear zone has been buckled about NW-trending axes to the present-day domed architecture.

Meatiq dome encompasses three granite plutons; Um Baanib, Abu-Ziran, and Areiki intrusions (Fig.1c) which belong to distinct tectonic stages. These plutons account for nearly 50% of the total volume of exposed rocks in the dome with a suspected higher percentage in the subsurface. Um Baanib pluton is the largest intrusion in the dome. It is exposed in the core of Um Baanib antiform as an oval-shaped pluton with NW- trending axis (Fig.1c). Rocks of the pluton are intensely deformed granites and granodiorites with a gneissose appearance and pronounced penetrative ductile fabric. Abu Ziran Pluton is a large pluton that include all intrusive masses of tonalite and granodiorite in the central and southern parts of Meatiq dome (Fig.1c). These granites exhibit strong to mild mylonitic fabrics, mostly intensified near the contacts with country rocks (Sturchio et al., 1983). The last intrusions are the alkali-feldspar granites which are best represented by the circular Arieki pluton.

Thanks to a wealth of geochronological data, the magmatic history of Meatiq dome is well constrained, but the relationship among magmatic and structural phases are still debated. Um Baanib deformed granites give a U–Pb crystallization age of about 630± 2 Ma (Andresen et al., 2009), which is comparable with the Rb-Sr age (626 ± 2 Ma) obtained by Sturchio et al., (1983). These ages were interpreted by some authors to reflect a pre-orogenic emplacement (e.g., Fritz et al., 1996; Loizenbauer et al., 2001; Andresen et al., 2010), while other suggested a syn-orogenic emplacement (e.g., Khudeir et al., 2008; Andresen et al., 2009; Mohammad et al., 2020). U-Pb ages of Abu Ziran pluton ranges between 614 ± 8 Ma (Stern and Hedge 1985) to 606 ± 1 Ma (Andresen et al., 2009). The emplacement of Abu Ziran pluton was accepted by most workers as syn-tectonic. However, opinions concerning the prevailing tectonic regime associated with emplacement vary from extensional (Fritz et al., 1996, 2002; Hamdy et al., 2017) to compressional (Sturchio et al., 1983). Areiki pluton is fairly intact, unaffected by penetrative deformation fabrics, and only dissected by brittle normal faults. Data from Arieki pluton reveal crystallization ages of about 591 ± 3 Ma using U–Pb TIMS method (Andresen et al., 2009), and 579 ± 6 Ma using Rb–Sr dating (Sturchio et al., 1983). It was interpreted as a post-collision intrusion, and its age used to bracket the ceasing of compressional processes (e.g., Andresen et al., 2010).

The structural and cooling history of Meatiq dome were constrained from ^{40}Ar–^{39}Ar dating of white mica and hornblende crystals from mylonitic rocks (Fritz et al., 2002). The activity of the proposed sinistral strike-slip shear zones and extensional shear zones bordering Meatiq dome has been dated by syn-kinematic white-mica that gave ages of 588 Ma and 595 Ma (Fritz et al., 1996). These dates are comparable with cooling ages of Fritz et al., (2002) which derived from hornblende (579–587 Ma) and muscovite crystals (582 Ma) and reflects cooling from high temperatures (exceeding 500° C) down to about 350° C.

3. Structural framework of Meatiq shear zone

3.1 Field observations and structural data

Meatiq dome exposes an intensely deformed succession of mylonitic metasediments and deformed granites that are collectively known as Meatiq Succession (Hassan et al., 2017) or Abu-Fannani thrust sheet (Andresen et al., 2010; Johnson et al., 2011). These rocks are penetratively foliated, banded and intensely folded as a result of strong ductile deformation. The widespread existence of fabrics and structures with clear monoclinic asymmetry implies a strong non-coaxial component of deformation. These ductile fabrics were interpreted as vestiges of a major thrust shear zone that has been imposed by the earlier phase related to island-arcs accretion and nappes stacking (Andresen et al., 2010). In this section, we will focus only on the structural features of MSZ and its relationships to Abu Ziran pluton. Detailed structural architecture and kinematics of this shear zone are beyond the scope of the present work.

The dominant fabrics in MSZ are the pronounced mylonitic foliation, stretching mineral lineation, mesoscale folds, and ductile shear zones. The mylonitic foliation (Sm_1) is defined by the preferred orientation of mica and hornblende grains and stretched quartz ribbons. A pervasive mineral stretching lineation (L_1) is widely noted along foliation planes and it is marked by the alignment of elongated mica and amphibole aggregates and stretched garnet porphyroblasts. The lineation is mostly trending NW-SE, which is remarkably constant along the shear zone, while mylonitic foliation generally follows the orientation of macroscopic folds. Sheared quartz veins are significant mesoscopic structures in MSZ. They show boudinage and pinch- and swell structures with a prominent extension parallel to the mylonitic foliation (Figs.2a, b, c& d). Some of these boudinage veins form asymmetrical sigmoidal-shaped lensoidal boudin trains with distinctive pressure shadows (Figs.2a, b). Mylonitic foliation and banding are disturbed by the formation of folds, crenulation cleavages and shear bands. Different generations of folds were examined in the Meatiq dome.

The most prominent fold generation is the NE-trending, tight to isoclinal folds with sub-horizontal axes (Fig.2 e, f). These folds are mostly well-developed in the quartzo-feldspathic rocks (Fig. 2g). They mostly exhibit an NW-ward vergence which is compatible with a top-to-NW tectonic transport (Fig.2 g, h). In zones with high shear strain near the contacts with ophiolitic nappes, most of these folds are completely transposed and are hardly recognizable. The second fold generation is gentle upright folds with NW-trending axes that fold the earlier ductile fabric. Mesoscopic kinematic indicators are frequent in MSZ and include S-C fabrics, shear bands, asymmetric boudins and intrafolial folds. They are kinematically consistent with an overall top-to-NW sense of shear.

The strain changes dramatically along the shear zone and intensifies close to the structural contacts between different rock varieties or along the borders of granitic sheets probably due to thermal softening. However, detailed discrimination of low- and high- strain domains is still a challenge in the Meatiq dome due to the lack of detailed structural mapping. Andresen et al., (2009) interpreted the magmatic pulse of Abu Ziran pluton and similar intrusions as a syn-tectonic lenses which emplaced along the sub-horizontal shear zone, and they used their crystallization age to constrain the time of shearing event. This stage of deformation/magmatism was accompanied by amphibolite facies metamorphism in the mylonitic metasediments and greenschist facies metamorphism in the ophiolitic nappes.

3.2 Microstructures

The microstructural analysis of the mylonitic varieties of MSZ indicates dominant crystal plastic deformation, controlled by a strong non-coaxial strain component. Tectonites of MSZ exhibit a broad range of microstructures due to variation in lithology, strain intensity and degrees of strain localization. In pelitic schists and phyllonites, the foliation is marked by the strong preferred orientation of amphibole and mica aggregates (Fig.3a), while quartz and feldspar ribbons define the planar fabric in quartzo-feldspathic rock varieties.

Mylonitic quartzites exhibit strong grain shape foliation, delineated by elongated quartz-ribbons with highly sutured and serrated boundaries. The peak metamorphic assemblage is marked by sillimanite, garnet, biotite, and hornblende, which reflects high metamorphic conditions, comparable with the peak of M2 phase identified by Neumayr et al., (1998). Three different generations of garnet porphyroblasts were observed in the thin section. The first one is represented by elongated, rod-shaped garnet crystals that are approximately parallel to the trace of the foliation and form a pervasive stretching lineation in some mica-rich varieties. The second generation is represented by elliptical to irregular-shaped garnet crystals with highly curved quartz inclusion trails marking an s-shaped internal foliation (Fig.3b). This geometry implies a syntectonic growth of some garnet porphyroblasts. The third generation is represented by euhedral to a subhedral crystal, cuts across the planar foliation and is probably related to metamorphic events post-dating the deformation (Fig.3c). The last category was observed in schist varieties near the contact with Abu Ziran pluton, which may reflect the growth in the contact aureole of the pluton after the ceasing of deformation.

Microscopic shear sense indicators are consistent with the observed mesoscopic ones and reflect top-to-NW tectonic transport. The common indicators are subcircular quartz porphyroclasts with distinctive pressure shadow that adopts a sigmoidal σ-type morphology (Fig.3d), S-C fabric (Fig.3e), and folded quartz veins and ribbons (Fig.3f).

4. Geology of Abu Ziran pluton

Abu Ziran intrusion comprises prominent detached masses of calc-alkaline granitoids (Fritz et al., 2014), covering an area of about 19 Km^2, and occupying the central and southern parts of the Meatiq dome. The outcrops of the pluton form low relief hills with distinctive spheroidal weathering and exfoliation. Abu Ziran pluton intrudes the amphibolite-facies schists and mylonites of Meatiq dome, and the overlying, greenschist-facies ophiolitic nappes, while it was intruded by a coarse-grained, fairly homogeneous, and undeformed alkali granite. Evidence for contact metamorphism accompanying the emplacement of the pluton was recognized in the southern ophiolitic rocks (Fritz and Phul 1996; Loizenbauer et al., 2001).

At the present level of exposure, the pluton crops out in three distinct, detached outcrops or domains (Fig.4). The first one forms a diamond-shaped outcrop that occurs in the central part of the Meatiq dome. The granite rests on the amphibolite-facies schists and mylonites, and its contact generally follows the attitude of the foliation in the country rocks. The second domain crops out in the entrance of Wadi Abu Ziran and forms a lowland terrain with a nearly triangular to subcircular-shaped exposure. It is demarcated from the western and eastern part by E-W and NW-SE trending normal faults respectively that juxtaposes the granite with the schists and mylonites. Farther to the south, the pluton intrudes the ophiolitic mélange parallel to the foliation and follows the attitude of the thrust faults. The third domain forms an elongated body along the main Qift-Quseir road and is trending in the WNW-ENE direction. The granite outcrop's length is about 10 Km, and the width varies from 800 to 50 m. Some strewn outcrops were mapped in the southern part of Um Baanib antiform, mostly extending parallel to the foliation in schists and mylonites.

Majority of the previous studies regarded only the southern outcrops and completely neglected the outcrop occupying the central part of the dome (Fritz et al., 1996, 2014; Loizenbauer et al., 2001). Other few contributions mapped the three outcrops, divided them into two distinct intrusions: Abu Ziran pluton for the intrusion exposed in Abu Ziran synform, and Abu Fannani pluton which incorporates the southern outcrops (Habib et al., 1985a, b; Neumayr et al., 1996; 1998; Andresen et al., 2010). Sturchio et al., (1983) deemed all outcrops as syn-tectonic tonalite intrusion without any further discrimination.

In the present study, the pluton was divided into three structural domains labelled A, B, and C domains. Domain A includes the outcrops of the central part of the dome, while B and C domains comprise the outcrops extending along the southern part of the dome (Fig.4). The composition of these different domain of the pluton is similar as evidenced from petrography, geochemistry, and remote sensing studies (Sultan 1984; Habib et al., 1985a, b; Sultan et al., 1987; Abdel-Rahman 2021). Nevertheless, Fritz et al., (1996, 2014) presented a different perception for Abu Ziran pluton as they interpreted the southern outcrops as two separate segments with distinct composition. They assumed an E-W magmatic differentiation from calc-alkaline chemistry in the west to alkaline chemistry in the east, which follows magmatic flow and variations in strain intensity. U-Pb zircon ages of 606 ± 1 Ma (Andresen et al., 2009), and 614 ± 8 Ma (Stern and Hedge 1985) were obtained from domains B& C respectively.

4.1 Field observations and structural data

4.1.1 Mesoscopic structures

Abu Ziran granitoids show conspicuous outcrop-scale magmatic layering, flow bands, and mafic schlieren, which are marked by melanocratic layers of biotite and hornblende, alternating with leucocratic domains rich in quartz and plagioclase (Fig.5a, b). Inside the schlieren, mafic minerals are oriented preferentially parallel to layer contacts. The layering mostly strikes parallel to the pluton's contacts and shares the same orientation of tectonic foliation in the wall rocks. Aligned plagioclase crystals of igneous origin clearly define magmatic lineation chiefly trending NW-SE. Fritz et al., (2014) pointed out that magmatic foliation is mostly parallel to the mylonitic foliation, and the long axes of magmatic crystals are aligned in E-W to WNW-ESE directions. Close to the pluton's contacts, magmatic fabrics are less pronounced and largely overprinted by intense and penetrative tectonic deformation.

Tectonic fabrics are represented by mylonitic foliation, well-developed S-C fabric, and NW-SE-trending mineral lineation. Foliation is defined by the preferred orientation of quartz ribbons, plagioclase and mica crystals, and reveals broad concordance with the enveloping wall-rock contacts. Stretched mafic enclaves are frequent in the southern part of the pluton, commonly associated with mylonitic granite varieties, and oriented NW-SE (Figs.5c, d). Sturchio et al., (1983) reported mafic enclaves with distinctive sigmoidal-shaped "enclave fish" aligned in a framework of well-developed S-C fabric and indicating apparent dextral shear sense. This pattern was interpreted as a clue for the top-to-NW tectonic transport (thrusting) that accompanied the pluton emplacement. A few sheared dykes of pegmatites and aplites are preserved locally, usually oriented parallel to mylonitic foliation (Fig.5e).

In general, the intensity of tectonic fabrics decreases toward the low-strain domains in the inner parts of the pluton. The ductile fabrics of the pluton are dissected by an array of brittle thrust faults, trending ENE-WSE and forming distinctive thrust duplexes (Figs.5f). Slip lineations along fault planes plunge 20 to 30° to the SSW (Figs.5g). In addition, the pluton is sliced with a set of variable oriented normal faults and fractures. These brittle extensional structures cut the magmatic and ductile fabrics in the granitoids and reveal the exposure of the pluton to multiple extensional phases after the ceasing of orogenic pulses.

4.1.2 Petrography and microstructures

The granitoid suit of the Abu Ziran pluton ranges in composition from quartz diorites, trondhjemite and tonalites to granodiorite. They comprise coarse-grained, hypidiomorphic rocks, essentially composed of plagioclase, quartz, biotite, and hornblende. Sericite, sphene, and opaques are the common accessory minerals. K-feldspar minerals are more common in granodiorite varieties and represented by microcline and perthite. Based on microstructural criteria, Abu Ziran granitoids exhibit a wide spectrum of deformation from mild deformation in the inner parts of the pluton to intense deformation along the contacts with wall rock (Fig.6). The southern outcrops of the pluton document a well-preserved transition from magmatic to solid-state fabrics.

4.1.2.1 Magmatic and sub-magmatic microstructures

Magmatic fabrics are well-discernible in the low-strain domains of the pluton, subjected to faint tectonic deformation. In these varieties, primary magmatic foliation is defined by the shape-preferred orientation of plagioclase crystals with euhedral tabular shape, albite twinning and oscillatory zoning (Fig.6a). The crystals are not significantly deformed or recrystallized, and clearly retain most of the magmatic nature. Some crystals exhibit strong sericitization which obliterate primary magmatic features (Fig.6b). The aligned tabular crystals surrounded by anhedral, non-deformed interstitial quartz grains and euhedral to subhedral mafic minerals (biotite and hornblende). Next to the intrusive contacts with alkali-feldspar granite, samples occasionally showing graphic and myrmekitic intergrowth textures in K-feldspar and plagioclase (Fig.6c).

These observed microfabrics reveal a melt-present magmatic flow with limited interactions among crystallized grains. Toward pluton's rims, the onset of ductile deformation microfabric on plagioclase and quartz marks the transition to a regime dominated by sub-magmatic microstructures. Plagioclase was partially recrystallized by bulging (BLG) and sub-grain rotation (SGR), however, it still retains the relicts of magmatic features (tabular-shape, zoning and twinning; Fig.6d). In addition, quartz grains occur as elongated grains with sutured boundaries or as small aggregates. These microstructural features are clues for ductile deformation and dynamic recrystallization through grain boundary migration (GBM) and subgrain rotation (SGR), which indicate deformation in the presence of melt (Paterson et al., 1989).

4.1.2.2 Solid-state microstructures

Solid-state deformation and dynamic recrystallization are obvious in the high-strain domains along the rim of pluton. The examined samples are characterized by local gneissification or typical high-grade mylonitic texture with ubiquitous strong oblique foliation (S), cut by well-developed horizontal shear bands (C-surfaces). S-foliation is defined by the alignment of mica, hornblende, and large plagioclase crystals, while C-surfaces are marked by arrangement of biotite aggregates and quartz subgrains (Figs. 6e, f). Near the margin of porphyroclasts, plagioclase is often corroded and recrystallized, mostly by sub-grain rotation, which imply high temperature deformation. They are usually sheared into S–C fabric or deformed into lozenge-shaped σ-type porphyroclasts, commonly defining a core- mantle microstructure (Fig. 6g). Quartz occurs as polycrystalline ribbons made up of recrystallized grains with lobate boundaries and elongated parallel to S and C planes (Fig. 6h), or as small grains and aggregates indicating grain size reduction by SGR (Figs. 6h, i). The observed kinematic indicators, including S-C fabrics, σ -type porphyroclasts, and stair stepping of the foliation around the porphyroclasts indicate top-to-NW movement sense the same as mylonites in the wall-rocks.

4.2 Structural analysis of Abu Ziran pluton

4.2.1 Domain A

This domain is located in the central part of the Meatiq dome, along the NW-trending synformal structure which is referred to as Abu Ziran synform. The main body of the pluton occurs as a diamond-shaped exposure, covers an area of about 10 km^2, and is roughly centered on the core of the synform (Fig.7). The pluton is accessed by two transects nearly sub-parallel to the synform axis; the N-S-trending wadi Abu Ziran east and the NW-trending wadi Abu Ziran west. In wadi Abu Ziran east, the granites occupying the uppermost parts of the valley slopes as a dipping sheet overlies the schist and mylonites and have an average dip of about 35° to the core of the synform (Fig.8a).

The floor of the pluton is mostly concordant to the country rocks, and exclusively parallel to the foliation in the wall-rock (Fig.8b). Intrusive contacts are generally sharp, and no evidence for forceful emplacement has been noticed. In wadi Abu Ziran west, the pluton is exposed along the valley slopes as low-relief hills. The orientation of the pluton's floor changes and dips gently about 25°-30° to the NE, which lends an overall synformal shape to the pluton contact. The valley runs along an NW-trending normal fault that cuts across the pluton. Abu Ziran pluton was invaded, with sharp intrusive contacts, by an elliptical plug of alkali granites.

The roof contact of Abu Ziran pluton is almost eroded over the entire extent of the exposure, except for an elevated ridge in the north, where both floor and roof contacts have been preserved along the structural boundary between mylonites and amphibolites, providing a natural cross-section of the entire pluton (Fig.8c). The pluton is exposed as an SW-ward dipping sheet-shaped intrusion that follows the orientation of wall rocks (Fig.8d). Close to the pluton contacts, the granite exhibits a local gneissification and well-developed mylonitic fabric with obvious plagioclase porphyroclasts and S-C fabric (Figs.8e, f). The country rocks are invaded with several sheet-intrusions of highly foliated granitoids, which are parallel to the pluton itself (Fig.8g). The southern tip of this domain is demarcated by several normal faults, trending NW-SE, N-S, and NE-SE. Some of these faults accumulate a vertical displacement up to 130m. Farther to the south, some strewn masses of the Abu Ziran granites are reported on the crests of high-relief ridges, mostly on footwall blocks of the normal faults, as topographic outliers. This reveals that the Abu Ziran pluton was extended southward and was subjected to intense erosion in the uplifted fault blocks.

Stereographic plots of S_1 foliation measurements in the country rocks define a well-defined bimodal clustering of poles and indicate symmetrical fold with axis trends S35°E (Fig.7c). The best fit π- great circle indicates a gentle plunging to the SE with an angle of about 5°. However, local changes in orientation are common near major normal faults, where the dip usually steepens due to dragging along the faults. The stretching lineation in mylonites mostly has a consistent, gentle NW-plunging orientation (Fig.7c). The geometry of the pluton in this domain was delimited as a sheet-shaped intrusion that has been folded, with the wall rocks, into a synformal structure, oriented NW-SE, and dissected by normal faults of various orientations, mostly NE-SW and N-S (Fig.7c).

4.2.2 Domain B

This domain is exposed intermittently as triangular to sub-circular, low-lying outcrops along the southern margin of the Meatiq dome (Fig.9). It is composed of granodiorite, which gradually changes to tonalites and quartz diorites near the pluton contacts (Fritz et al., 2014). The domain is bounded to the west and the northeast by N-S and NW-SE normal faults respectively, which juxtaposes Abu Ziran granites against the mylonites of the Meatiq dome and act as a structural boundary for this domain (Fig.9 a, b). The pluton's floor contact was almost not exposed, except for small remnants on the footwall of the western fault, which is dipping approximately 45° to the east due to the dragging associated with normal faulting (Fig.10a). The roof crops out along the southern limit of this domain, where the pluton is overlain by the ophiolitic nappes with a nearly concordant contact, dipping shallowly to the SE. The rocks near the pluton contacts are highly deformed, exhibiting a pronounced penetrative foliation and stretched mineral lineation (Fig.10b). In this domain, Abu Ziran granites are extensively intruded by the alkali granites with sharp contacts (Figs.10c, d &e). These intruding pink granitoids are undeformed and cut across the granitoids of Abu Ziran pluton, which may indicate a post-orogenic emplacement.
S_1 foliation trajectories in the country rocks reveal a fault-bounded synform with a shallow plunging to the SE. The stretching lineation along S_1 planes is mostly sub-horizontal and trends NW-SE, except for southern parts where lineation plunges shallowly SE. Farther to the east, Abu Ziran granites are exposed along the southern flank of Um Baanib antiform, along the contact between schists and ophiolitic rocks, and gradually fading out to the east. Some remnants of this pluton are locally preserved in the uplifted fault blocks, which, in turn, reflects a previous extension for the pluton over these rocks and subjected later to extensive erosion. Structural analysis of this domain suggests that it represents a subsided, fault-bounded portion of a larger sheet-shaped pluton, which was protected from the extensive erosion by the bounding mylonite and schists shoulders (Fig.9c, d).

4.2.3 Domain C

Abu Ziran granites in domain C exposed as an elongate, sheet-shaped igneous body strikes roughly WNW-ESE and can be traced along the Qift-Quseir road. The pluton documents a well-preserved roof and floor contacts with moderate south-ward dipping, concordant intrusive relationships with the country rocks and forms a distinctive sheet-shaped geometry (Fig.11).

The pluton attains a thickness of about 800 to 350 meters and decreases to about 50 meters near the contact with the Atalla shear zone.

In domain C, the sheet intrusion comprises, at different scales, separating small sheets which are connected through broken bridges and steps and separated by several screens of schists and mylonites. Completely isolated rafts and enclaves of country rocks occur in several localities and probably marks sites of sheets coalescing. The pluton floor is bounded to the north by a nearly E-W striking normal fault which juxtaposes the schists with the granites, while the roof of the pluton is demarcated by the sheared rocks near or along the thrust contact with ophiolites (Fig.11a). Relics of the pluton floor are also locally preserved on the hanging wall of the normal faults, where the pluton occurs as a sub-horizontal sheet overlies Abu Fannani schists and mylonites (Figs.11b, c).

S1 foliation in the country rocks exhibits a general S to SW dipping with angles up to 55°. Boudinage quartz veins and asymmetrical folds are common structural features near the pluton contacts and are kinematically consistent with top-to-NW transport. In addition, stretched mafic enclaves and xenoliths of amphibolites are widely noticed across this domain (Fig.11d). The stretching lineation along S1 planes is mostly sub-horizontal and trends NW-SE, except for southern parts where lineation plunges shallowly SE (Fig.11e). The pluton body was transected by multiple ductile shear zones manifested by domains of well-developed mylonitic foliation and S-C fabric, especially near pluton contacts.

The pluton in domain C was interpreted as a moderately, S- to SW-dipping complex sheet with a remarkable decrease of thickness to the east. The whole sheet occupies the hanging wall of the E-W oriented extensional fault, except for small remnants of the pluton that were preserved on the footwall of the fault, resting upon the mylonites and schist of the Meatiq dome.

5. Reconstructing the 3D geometry of the pluton

Following the investigation of syn-tectonic tonalitic intrusions in Meatiq dome, we tried to derive the geometry of these granitic intrusions and determining whether they represent separate synchronous intrusions or are remnants of a larger pluton was emplaced along MSZ and subjected to later tectonic processes and denudation. The three-dimensional form and the evolution of the pluton geometry has been deduced by combining geological information from the excellent exposures of both floor and roof contacts of the pluton along transects through and across the pluton in the different domain. In the investigation, the following points should be considered: (1) All of the examined tonalite and granodiorite intrusions detected in the Meatiq dome have a distinctive sheet-shaped geometry that was affected by later both ductile and brittle phases. (2) There is a clear concordance between the orientation of roof and floor contacts of the pluton and the ductile fabrics in the shear zone, where contacts are mostly parallel to the shear zone walls. (3) The pluton exposures are dramatically confined to localities where the contacts with the overlaying ophiolitic nappes are exposed. (4) Several small and strewn relics of Abu Ziran granitoids were reported on top of fault-bounded high-relief hills. Indeed, all these lines of evidence, along with reviewing previous literature, suggested with reasonable confidence that the separate domains of Abu Ziran intrusion are remnants of an earlier continuous pluton with a tabular sheet-shaped pluton that covered most of the western side of the Meatiq dome.

Abu Ziran pluton was mostly parallel to the contact Meatiq mylonites and overlying ophiolitic nappes, and to the tectonic fabrics in the MSZ. Detailed examination discloses that the pluton consists of smaller sheets, have been emplaced along closely spaced structural contacts, and coalesced through several bridges, connectors and steps into complex sheet-shaped intrusion. However, for simplicity, we will consider the pluton as a coherent sheet intrusion regardless of detailed internal architecture. The thickest part of the pluton is located on the southern side, and the gross thickness gradually tapers and vanishes toward the North. As a result of post-emplacement deformation (i.e., NE-SW shortening and multiple extension), the pluton's geometry has been markedly modified since intrusion and emerged to a more complex 3D shape (Fig.8b).

Two speculative cross-sectional oriented N-S and NW-SE correlate structural data from domain A to domains C and B respectively (Figs.12 a-e). The cross-sections clearly illustrate the sheet-shaped geometry of the pluton, and the concordant relationships of roof and floor contacts to country rocks. The previous continuity of the sheets was inferred based on the small vestiges of the Abu Ziran granite on the crests of high-relief ridges which mark the position of the eroded parts and verify the previous continuity of these detached sheets. Presently, the uneroded parts of Abu Ziran sheet-intrusion are only preserved locally, mainly in fault-controlled blocks. Our geometrical model, in turn, emphasizes a clear spatial correlation between magma emplacement and the geometry of the thrust shear zone.

The parallelism of the pluton contacts with the orientation of the mylonitic foliation suggested the usage of foliation attitude as a proxy to understand the complex architecture of the pluton, restore the pre-doming geometry, and infer the possible spatial extent that the pluton had before its erosion (Fig.12e, f). The pluton was approximately occupying most of the southwestern part of Meatiq dome and extends eastward to the mid of Um Baanib antiform as indicated by the limit of the pluton exposures along the southern flank of the dome (Fig. 13a). Four hypothetical cross-sections were constructed to illustrate the approximate geometry and extent of present-day and hypothetical parts of the pluton (Fig.13b). The pluton thickness decreases gradually in all directions except for the southern part. The accuracy of our model is limited to available structural data. However, despite limitations, this reconstruction introduces a preliminary envision about the initial extent and size of the pluton.

Previous studies reported several tabular and sheet-like intrusions on other parts of Meatiq dome which are beyond the studied area. Habib et al., (1985b) described a small, inclined lens of quartz monzodiorite exposed in the northwestern corner of the Meatiq dome along wadi Um Esh. These sheets trends NW-SE, dips to the W, and attains length up to 3 km and thickness about 400 m. Also, they invaded the enveloping mylonites and concordantly with sharp intrusive contacts. Similarly, Sturchio (1983) and Andresen et al., (2009) documented several numbers of small, concordant sheets and lenses of tonalites and quartz diorite along the eastern limb of Meatiq dome, which exhibit intense to mild deformation and localized mylonitization near the lens margins. Geochronological data estimates of two of these small lenses reveal crystallization ages of (609 to 605 Ma; Andresen et al., 2009), which are similar to the age of Abu Ziran pluton. These sheets can be interpreted as intrusions, correlatable with Abu Ziran pluton, and emplaced on the northwestern and eastern flanks of Meatiq dome, or as potential extensions for Abu Ziran pluton itself toward the east and northwest.

6. Discussion and implications

6.1 Room problem in compressional settings

Emplacement of syn-tectonic intrusions along shear zones in thrust-dominated regimes represents a subject of debate in modern structural geology. In the earlier stages of research regarding the control of geological structures on magmatism, there is a preconception that compressional conditions in fold-thrust belts are expected to prevent the ascent and emplacement of magma through the crust (Hutton 1996). However, this is at odds with the fact that most granite plutons and intrusions primarily occur in convergent orogenic belts (e.g., Hutton, 1996; Barbarin, 1999). In addition, several unequivocal examples of plutons emplaced along thrust faults and shear zones have been documented in several orogenic belts (e.g., Blumenfeld and Bouchez, 1988; Crawford and Crawford 1991; Tobisch and Paterson 1990; Hutton and Ingram, 1992; Karlstrom et al. 1993; Ingram and Hutton, 1994; Rosenberg et al., 1995; Collins and Sawyer 1996; Searle 1999; Blenkinsop and Treloar 2001; Kalakay et al., 2001; Spanner and Kruhl 2002; Aranguren et al., 2003; Musumeci et al. 2005; Ferre´ et al., 2012), which indicates that spaces required for emplacement are created in such regimes somehow. This Lack of clear comprehension for the mechanisms of the room origin required for magma emplacement in these space-denying regimes was one of the main problems confronting the geologists.

Several models were proposed for explaining the mechanisms of room creation and magma emplacement at different crustal levels under both brittle and ductile conditions. The simplest proposition was introduced by Ingram and Hutton (1994), where they suggested that some plutons in a contractional environment chiefly emplace along the thrust flats, which act as dilational bends in the thrust system (Fig. 14a). In case of high-angle reverse faults, they envisaged that magmatic wedging mechanism (Anderson, 1951) enhanced by rock anisotropies, structural weaknesses along faults and shear zones, and repeated internal diking would be able to overcome the orogenic compressional stresses and allow the magma ascent and emplacement (Fig. 14b; Ingram and Hutton 1994). Vigneresse (1995) disclosed that magma emplacement always occurs in locally extensional sites along faults and shear zones, regardless of the regional stress state. A new model was proposed by Rosenberg et al., (1995), based on observations from Bergell pluton, which stated that regional shortening at deeper crustal levels squeezes the granitic melt and induces its vertical movement and escaping to upper structural levels in the crust (Fig. 14c). Hutton (1996) stated that emplacement processes vary with depth in orogenic belts and tried to formulate a general scheme illustrating the diverse ways of space problem solving across the different crustal domains. He suggested that the rocks in the lower crust behave as weak ductile materials, thus the strain of ascent and emplacement of plutons will be experienced regionally, and the space problem is regionally solved. In contrast, the space problem in the middle crust is solved locally via tensional and dilating sites in and around faults and shear zones. At higher crustal levels, emplacement is influenced by the closeness to the earth's surface, and spaces are dominantly created by uplift and brittle deformation of the free surface such as cauldron subsidence, magmatic stoping, ring faulting, and roof uplift.

In the last two decades, the growing interest has been devoted to understanding the mutual interplay of the magmatic and deformation processes in the fold and thrust belts. Kalakay et al., (2001) demonstrated the clear spatial correlation between pluton emplacement and the top of the frontal thrust ramp. In their ramp-top emplacement model, they highlighted the integrated roles of dilational steps at top of ramps and the antithetic back-thrust faults in facilitating the emplacement of magma in shallow-seated thrust systems (Fig. 14d). Galland et al., (2008) compared data from case studies in the Andes mountains and the United States and results from experimental modeling to emphasize that magma in the fold and thrust belts can ascend via the thrust faults and be emplaced mainly as sills or sheet intrusions mostly along horizontal segments. In addition, the emplaced magma influences the pattern of deformation at upper crustal levels. Ferre´ et al., (2012) reviewed several case studies for plutons emplaced in compressional settings and integrated these data with results from the analogue modeling to establish a more sophisticated scheme for the mutual relationship between granite plutons and shear zones. They confirm the strong spatial correlation between the geometry of emplaced syn-tectonic plutons and thrust shear zones. Moreover, they emphasized the effect of time relationships among magmatism and deformation on the shape of the mode of pluton growth. Pre-kinematic plutons are not spatially controlled by the geometry thrust faults, and usually have a non-elongated geometry that has been squeezed during ongoing deformation. Unlikely, syn-kinematic plutons are structurally controlled intrusions that have migrated laterally along the thrust faults and accumulated either along flats or hanging-wall anticlines (Fig.14e, f). The post-tectonic intrusions track the pre-existing structures in the thrust systems, which exerts a significant control on the melt migration and emplacement (Fig. 14g). The recent contributions on the architecture magma plumbing system, drawn from field studies and 3D seismic data, revolutionized our view to the geometry of their components (sheet-shaped intrusions) and the role of pre-existing anisotropies on their morphology and emplacement mechanism (e.g., Schofield et al., 2012; Magee et al.,2016, 2019; Eide et al., 2017; Köpping, 2022; Köpping et al., 2022).

In conclusion, it is affirmed from both experimental investigations and natural that there is a strong spatial relationship between emplacement of syn- and post-kinematic granite plutons and the geometry of thrust shear zones and faults (Ferre´ et al., 2012 and references therein). In mid- and upper-crustal levels, regardless of the proposed mechanism, horizontal segments in the thrust system (i.e., flats), and hanging-wall anticlines (fault-bend folds) constitute the main sites for emplacement and localization of syn-tectonic plutons, while ramps in thrust systems act as conduits for melt migration and ascent (Ferre´ et al., 2012). The geometry of a pluton reflects the structural interaction between internal magma parameters (composition of magma, viscosity, density, magmatic pressure) and external parameters (regional stress, inherited discontinuities, rheology of wall rocks) and contains information that summarizes each step in its formation (Petford et al. 1997; Breitkreuz and Petford 2004). They generally vary from sheet-intrusions and sills which grade by in-situ inflation into laccoliths (Burchardt 2009; Bunger and Cruden 2011).

Interestingly, experiments, numerical simulations, and case studies from numerous orogens demonstrate the importance of subhorizontal rheological discontinuities for trapping the magma and forming tabular intrusions (Roman-Berdiel et al., 1995, 1997; Watanabe et al. 1999; Musumeci et al. 2005; Galland et al., 2006, 2007). These rheological boundaries act as strong barriers for ascending melt (Hogan et al., 1998; Gerya and Burg 2007; Galland et al., 2009; Mazzarini et al., 2010). Moreover, it is widely accepted that the geometry of sheet intrusions is controlled by the orientation of principal stress axes during emplacement (Anderson, 1951; Muirhead et al., 2015: Magee et al., 2019). The sheet intrusion walls are orienting parallel to the $\sigma1$-$\sigma2$ plane and perpendicular to $\sigma3$, and thus providing a record of syn-emplacement stress conditions. The orientation of principal stresses in the compressional regime usually induces the opening of horizontal fractures and with vertical extension (parallel to the least principal stress $\sigma3$), that enhances the accommodation of the ascending magma along horizontal flat segments (Sibson 2003; Ferre´ et al., 2012)

6.2 Emplacement model of Abu Ziran pluton

Based on the results of present study, a new emplacement model for Abu Ziran pluton was proposed. Our arguments arise from the examined field relationships, structural analysis of Abu Ziran pluton, and associated brittle-ductile fabrics in host rocks, which implies a close genetic relation between shear zone activity and pluton emplacement. At the time of emplacement, MSZ was comprising a nearly sub-horizontal segment which interpreted as a flat along a large-scale along thrust shear zone placing ophiolitic nappes upon the thick mylonitic metasedimentary succession of Meatiq dome (Sturchio et al., 1983; Mohammad et al., 2020).

The field and microstructural investigations point to thrust (top-to-NW) kinematics of MSZ. Deformation conditions in MSZ were dominantly ductile at the lower structural levels and switched gradually to brittle-ductile deformation in the upper levels near the contacts with ophiolitic nappes. Abu Ziran pluton was emplaced as a tongue-shaped complex sheet intrusion of quartz diorite, tonalite, and granodiorite during the late Neoproterozoic at about ~ 606 Ma (Andresen et al., 2009). Hornblende crystallization pressure of 4-6 kbar reported from the southern domains of the pluton suggests emplacement depth of ~15-20 km (Fritz and Puhl 1996; Fritz et al., 2014).

The melt injection was chiefly localized at or near the contact between mylonitic metasediments and the overlying ophiolitic nappes, and no signs were observed for the accommodation of this magmatic pulse at the lower structural levels (Fig. 15a). The pluton documents a spectrum of deformational features varies from magmatic deformation in the inner part to sub-magmatic and solid-state deformation at the contacts with the shear zones. Magmatic foliation is parallel to the strike of pluton contacts and tectonic fabric in the host rock (Figs. 15b, c). Macroscopic and microscopic features from the pluton reveal also a top-to-NW shear sense which is consistent with kinematic in the host rocks and underlines the connection between deformation in MSZ and the pluton emplacement (syn-kinematic). The obvious partitioning of deformation in the pluton into sub-magmatic to solid-state microstructures along the rim, and magmatic deformation in the inner parts may implies that cooling rates exceeds the tectonic rates (e.g., Papeschi et al., 2022) and supports emplacement during the waning stages of the shear zone activity (Miller and Paterson 1994). The absence of any magmatically-induced strain in wall-rock suggests that accommodation of the pluton was governed by passive emplacement mechanisms.

We postulate that several factors interacted, and controlled the room creation, pluton geometry and mode of emplacement. The first element is the pre-existing anisotropies, especially thrust faults and foliations. Inherited damage zones associated with thrust faults provide a preferential pathway for magma flow and emplacement. The recognition of some connecting structures preserved in the pluton like broken bridges, rafts and bridge xenoliths (Fig.11b), signifies the role of inherited structures, and stands that the pluton was not emplaced as a single continuous sheet intrusion, but evolved through the overlapping and linkage of multiple discontinuous segments (Walsh et al., 2003; Eide et al., 2016; Magee et al., 2019). Yet, a full characterization of these geometrical forms is still lacking and requires a more detailed study involving high-resolution mapping of their geometry, size, and spatial relationships. The second factor is the orientation of principal stresses in the compressional regime (horizontal $\sigma 1$ and vertical $\sigma 3$), which induces the vertical extension orthogonal to the shear zone and facilitates the flow of melt along the flat segment and pluton inflation (Fig.15d). In addition, the localization of Abu Ziran intrusion near or along the thrust contact in upper structural levels, reveals that the melt emplacement was affected by the rheological contrast between rigid ultra-mafic and mafic ophiolitic rocks and ductile mylonitic metasediments. This sharp contrast in competency acted as a rheological trap promoted magma arrest and favored horizontal spreading of melt (Fig.15e).

Magma probably has ascended along one or more feeder dykes, not exposed at the present erosion level, or through a non-exposed ramp along the thrust shear zone that may have served as magma conduits. As the magma reaches structural weaknesses near or along the horizontal fault zone, the magmatic flow has been flipped from vertical to horizontal movement parallel to the shear zone walls. After emplacement, and as a consequence of later shortening and extensional events, the pluton has been subjected to intense folding and faulting, resulting in widespread denudation and local preservation of the pluton as detached outcrops restricted to fault-bounded, subsided blocks.

6.3 Spatio-temporal evolution of pluton geometry

Abu Ziran pluton documents a complex, multi-stage deformation history that covers a wide time extending from Ediacaran to Tertiary. A new scheme for the spatio-temporal evolution of the pluton architecture since the emplacement to final exhumation. Based on a combination of data from structural analysis supported by published geochronology and geochemistry datasets, we suggest the following scenario for the evolution of the pluton. The structural history of the pluton witnessed four main stages of deformation. The earlier three stages were associated with Gondwana amalgamation and post-amalgamation processes (650-550 Ma). The fourth one is associated with the Phanerozoic rifting and opening of the Red Sea.

The D1 phase was associated with the island-arcs accretion tectonic episode. The fabrics and structures of D1 are manifested by penetrative mylonitic foliation (S1), NW-plunging stretching lineation (L1), and the NE-trending, tight to isoclinal recumbent folds (F1). Structural analysis of D1 structures suggested that they have been initiated in a thick, extensive sub-horizontal shear zone (MSZ), and constitute a ductile to brittle-ductile root for the ophiolitic thrust nappes. Kinematic indicators are mostly parallel to the stretching lineation and point to a regional top-to- NW tectonic transport. The prevailing metamorphic conditions coeval with D1 were amphibolite-grade metamorphism in the mylonitic metasediments (530-690°C at 5.8-8 kbar; Neumayr et al., 1998) and greenschist facies metamorphism in the ophiolitic nappes and mélange (350-540°C at P <4 kbar; Neumayr et al., 1998). The D1 phase was accompanied by a calc-alkaline magmatic pulse, which is represented by granites of Abu Ziran pluton and has a geochemical affinity similar to the volcanic-arcs magmatism (e.g., Mohamed and Abdel Ghani 2000; Fritz et al., 2014). The intrusion is emplaced as a sub-horizontal sheet-shaped pluton, usually parallel to foliation and shear zone walls. The age of deformed varieties of Abu Ziran pluton was used to constrain the ceasing of MSZ to about 605.8 ± 0.9 Ma (Andresen et al., 2009). However, the dated quartz-diorite and tonalite lenses from the eastern flank of Meatiq dome may expand the timing of this magmatic pulse to up to ~ 609 Ma (Andresen et al., 2010). Contrary to doubts cast by Fritz et al., (2014), who proposed an emplacement in an extensional shear zone with top-to-S shear sense, field observations and results of structural analysis contrast with their model and are strongly consistent with the kinematics of a thrust shear zone, accompanying transport of ophiolitic nappes (e.g., Sturchio et al., 1983; Mohammad et al., 2020).

D2 was the main contributing phase in the formation of the Meatiq dome. In this stage, the deformation has been switched to a nearly NE-SE shortening probably associated with the terminal oblique collision of East- and West-Gondwana at about 600 Ma (Abu Sharib et al., 2019; Mohammad et al., 2020). This phase involved the formation of the map-scale NW-trending folds and NW-SE striking thrust faults in Meatiq dome. Nevertheless, this phase is not associated with any penetrative fabric, at least in Meatiq area. As a consequence of the shortening, the MSZ has been folded, and D1 fabrics and structures were reoriented. Poles to S1 foliation defines two doubly plunging antiforms with a synformal structures between them. In this stage, the complex, sheet-shaped Abu Ziran pluton was subjected, as the encircling MSZ, to folding around NW-SE folding axis. This phase is assumed to be associated with the oblique convergence and final collision of East and West Gondwana that culminated at ca. 600-590 Ma (Andresen et al., 2010; Johnsen et al., 2011; Abu-Sharib et al., 2019). The activity of the NSS in the CED was associated with this phase of deformation.

After the ceasing of orogenic collision about 596-590 Ma (Andresen et al., 2009, 2010), the ANS was subjected to an extensional phase which is probably related to gravitational collapse of the orogenic belt and manifested by the wide-spread E- to NE- trending normal faults in central and northern parts of Eastern Desert of Egypt (Stern and Hedge 1985; Andresen et al., 2010; Stern and Ali 2020). During this phase, the Meatiq dome was transected by several, NE-SW-oriented normal faults.

Unlike the claims suggested by several authors that Meatiq dome and similar metamorphic complexes were fully exhumed at the late and post-orogenic process (e.g., Fritz et al., 1996, 2002; Hamdy et al., 2017), there is no evidence for full exhumation of amphibolite-facies rocks of Meatiq dome was achieved during Ediacaran. The thermochronological constraints introduced by Fritz et al., (2002) reveals that the cooling of Meatiq dome from high temperatures (exceeding 500° C) down to about 350° C at 579–587 Ma. We speculate that Meatiq dome underwent only a partial exhumation under the NE-SW shortening and the subsequent NW-SE extension. The full exposure of the dome was accomplished during the Phanerozoic extensional phases (D4) at Cretaceous (ENE-WSW extension) and Tertiary (NE-SW extension), that resulted in intensive denudation for the Precambrian rocks and overlying sedimentary cover. This is evidenced from the presence of WNW-ESE and NW-SE striking normal faults that slices the rocks of Meatiq dome and demarcate some of the domains of Abu Ziran pluton. About 5 km of phanerozoic overburden were stripped off from the Precambrian rocks along the Red Sea coast (Bojar et al., 2002). During these subsequent extensional phases through late-Precambrian, Cretaceous and Tertiary, Abu Ziran pluton has been dissected with a wide-range of normal faults that sliced the folded pluton.

The extensive Phanerozoic extensional pulses resulted in erosion of the portions of the pluton resting on the footwall of fault blocks, and only the fault-bounded subsided segments were protected from erosion by the adjoining durable mylonite and schists ridges. However, remnants of the pluton are still locally preserved on some uplifted, fault-bounded ridges which clues previous continuity of the pluton. Although this complex structural history blurred the original geometry of the pluton, remnants of the original sheet-shaped geometry can still be discerned in places. The present model, derived from structural analyses of the pluton, represents a new attempt to extend the Abu Ziran pluton beyond the currently accepted outcrops at the southern margin of the Meatiq dome, as well as aiding in a more comprehensive understanding of the pluton's geometry and evolution with time. Further constraints from geochemistry and thermochronology are required for an improved grasping of the magmatic and exhumation history of the pluton.

7. Conclusions

The Neoproterozoic Abu Ziran pluton is a typical example of syn-kinematic plutons emplaced along active shear zones in compressional tectonic settings. Owing to its well-exposed contacts and clearly documented structural relations, Abu Ziran pluton represents an excellent case-study to understand the 3D geometry of syn-kinematic plutons emplaced in thrust shear zones and constraining the factors contributing to their final architecture. The present study synthesizes results from field work, microstructures and remote sensing to characterize the nature of the deformation in both the pluton and the host rocks. The integration of results from different scales of observations allows the precise reconstruction of the pluton geometry and evolution in space and time.

The chief conclusions of our model can be drawn as follows: (1) the pluton was emplaced along thrust shear zone (MSZ) under ductile to brittle-ductile conditions, and has a clear tabular, sheet-shaped geometry that tapers to the N, and a sub-horizontal orientation that follows MSZ. (2) the pluton occupying the upper structural levels of MSZ near or along the thrust contact between ophiolitic nappes and mylonitic metasediments. (3) The pluton emplacement was principally passive, and the space required for emplacement and the geometry of the pluton was controlled mainly by the deformational processes operated in the shear zone, enhanced by the orientation of principal stresses. The rheological contact between ophiolitic nappes and mylonitic schist acted as a barrier that impeded the rise of ascending magma, causes magma arrest, and triggered lateral spreading and emplacement. (4) The melt may have ascended mainly either along unexposed feeder dyke(s), or via the inclined ramps in the thrust shear zone. (5) the pluton is made up of several deformed sheets, which were emplaced parallel to anisotropies along the shear zone (thrust faults and foliations), overlapped with each other, and linked via several broken bridges.

Since emplacement, the pluton has been subjected to several deformation phases that resulted in great modification on its geometry. During the late Neoproterozoic NE-SW shortening, the sheet-shaped pluton was subjected to folding and thrusting. Later the pluton was disturbed by subsequent pulses of extensional tectonics during Phanerozoic. By Miocene, the Precambrian basement of the ANS underwent intense exhumation and denudation which eroded all the parts of Abu Ziran Pluton, except subsided, fault-bounded blocks which survived from erosion thanks to adjacent durable shoulders. This complex structural history of Abu Ziran pluton blurred the original geometry and controlled its present-day mysterious architecture. The results of the present study introduce supportive evidence for the current view regarding the syn-kinematic plutons geometry and emplacement mechanisms along thrust shear zones.

8. References

Abd El-Wahed, M. A. (2008). Thrusting and transpressional shearing in the Pan-African nappe southwest El-Sibai core complex, Central Eastern Desert, Egypt. Journal of African Earth Sciences, 50(1), 16-36.

Abd El-Wahed, M. A. (2010). The role of the Najd Fault System in the tectonic evolution of the Hammamat molasse sediments, Eastern Desert, Egypt. Arabian Journal of Geosciences, 3(1), 1-26.

Abdeen, M. M., & Greiling, R. O. (2005). A quantitative structural study of late Pan-African compressional deformation in the Central Eastern Desert (Egypt) during Gondwana assembly. Gondwana Research, 8(4), 457-471.

Abdel-Rahman, A. (2021). Petrogenesis of a rare Ediacaran tonalite–trondhjemite–granodiorite suite, Egypt, and implications for Neoproterozoic Gondwana assembly. Geological Magazine, 158(4), 701-722. doi:10.1017/S0016756820000795

Ali, K., Andresen, A., Manton, W. I., Stern, R. J., Omar, S. A., & Maurice, A. E. (2012). U–Pb zircon dating and Sr–Nd–Hf isotopic evidence to support a juvenile origin of the~ 634 Ma El Shalul granitic gneiss dome, Arabian–Nubian Shield. Geological Magazine, 149(5), 783-797.

Anderson, E. M. (1951). The Dynamics of Faulting and Dyke Formation with Applications to Brittan, Edinburgh, Oliver and Boyd.

Andresen, A., Augland, L. E., Boghdady, G. Y., Lundmark, A. M., Elnady, O. M., Hassan, M. A., & El-Rus, M. A. (2010). Structural constraints on the evolution of the Meatiq gneiss dome (Egypt), East African orogen. Journal of African Earth Sciences, 57(5), 413-422.

Andresen, A., El-Rus, M. A. A., Myhre, P. I., Boghdady, G. Y., & Corfu, F. (2009). U–Pb TIMS age constraints on the evolution of the Neoproterozoic Meatiq Gneiss dome, Eastern Desert, Egypt. International Journal of Earth Sciences, 98(3), 481-497.

Aranguren, A., Cuevas, J., Tubia, J. M., Román-Berdiel, T., Casas-Sainz, A., & Casas-Ponsati, A. (2003). Granite laccolith emplacement in the Iberian arc: AMS and gravity study of the La Tojiza pluton (NW Spain). Journal of the Geological Society, 160(3), 435-445.

Bennett, J. D., & Mosley, P. N., (1987). Tiered-tectonics and evolution, E Desert and Sinai, Egypt. In: Matheis, G., Schandelmeier, H. (eds.) Current Research in African Earth Sciences. Balkema, Rotterdam, pp 79–82.

Bentor, Y. K. (1985). The crustal evolution of the Arabo-Nubian Massif with special reference to the Sinai Peninsula. Precambrian research, 28(1), 1-74.

Blenkinsop, T. G., & Treloar, P. J. (2001). Tabular intrusion and folding of the late Archaean Murehwa granite, Zimbabwe, during regional shortening. Journal of the Geological Society, 158(4), 653-664.

Blumenfeld, P., & Bouchez, J. L. (1988). Shear criteria in granite and migmatite deformed in the magmatic and solid states. Journal of Structural Geology, 10(4), 361-372.

Bojar, A. V., Fritz, H., Kargl, S., & Unzog, W. (2002). Phanerozoic tectonothermal history of the Arabian–Nubian shield in the Eastern Desert of Egypt: evidence from fission track and paleostress data. Journal of African Earth Sciences, 34(3-4), 191-202.

Bregar, M., Bauernhofer, A., Pelz, K., Kloetzli, U., Fritz, H., Neumayr, P. (2002). A late Neoproterozoic magmatic core complex in the Eastern Desert of Egypt: emplacement of granitoids in a wrench-tectonic setting. Precambrian Res. 118, 59–82.

Breitkreuz, C., & Petford, N. (Eds.). (2004). Physical geology of high-level magmatic systems. Geological Society of London.

Brown, M., & Solar, G. S. (1998). Granite ascent and emplacement during contractional deformation in convergent orogens. Journal of Structural Geology, 20(9-10), 1365-1393.

Brown, M., Rushmer, T., & Holness, M. B. (1997). The role of deformation in the movement of granitic melt: views from the laboratory and the field. Deformation-enhanced fluid transport in the Earth's crust and mantle, 8, 111-144.

Bunger, A. P., & Cruden, A. R. (2011). Modeling the growth of laccoliths and large mafic sills: Role of magma body forces. Journal of Geophysical Research: Solid Earth, 116(B2).

Burchardt, S. (2009). Mechanisms of magma emplacement in the upper crust (Doctoral dissertation, Niedersächsische Staats-und Universitätsbibliothek Göttingen).

Cao, S., & Neubauer, F. (2016). Deep crustal expressions of exhumed strike-slip fault systems: Shear zone initiation on rheological boundaries. Earth-Science Reviews, 162, 155-176.

Collins, W. J., & Sawyer, E. W. (1996). Pervasive granitoid magma transfer through the lower–middle crust during non-coaxial compressional deformation. Journal of Metamorphic Geology, 14(5), 565-579.

Crawford, M. L., & Crawford, W. A. (1991). Magma emplacement in a convergent tectonic orogen, southern Revillagigedo Island, southeastern Alaska. Canadian Journal of Earth Sciences, 28(6), 929-938.

D'lemos, R. S., Brown, M., & Strachan, R. A. (1992). Granite magma generation, ascent and emplacement within a transpressional orogen. Journal of the Geological Society, 149(4), 487-490.

Davidson, C., Hollister, L. S., & Schmid, S. M. (1992). Role of melt in the formation of a deep-crustal compressive shear zone: The MaClaren Glacier Metamorphic Belt, south central Alaska. Tectonics, 11(2), 348-359.

Davies, F. B. (1982). Pan-African granite intrusion in response to tectonic volume changes in a ductile shear zone from northern Saudi Arabia. The Journal of Geology, 90(5), 467-483.

de Wit, M. J., Armstrong, R., Hart, R. J., & Wilson, A. H. (1987). Felsic igneous rocks within the 3.3-to 3.5-Ga Barberton greenstone belt: High crustal level equivalents of the surrounding tonalite-trondhjemite terrain, emplaced during thrusting. Tectonics, 6(5), 529-549.

Eide, C.H., Schofield, N., Jerram, D.A. & Howell, J.A. (2017). Basin-scale architecture of deeply emplaced sill complexes: Jameson Land, East Greenland. J. Geol. Soc., 174, 23-40.

El Gaby, S., List, F. K., & Tehrani, R. (2017). The basement complex of the Eastern Desert and Sinai. In The geology of Egypt (pp. 175-184). Routledge.

El-Gaby, S. (1988). Geology, evolution and metallogenesis of the Pan-African belt in Egypt. The Pan-African belt of the northeast Africa and adjacent areas, 17-68.

El-Gaby, S., El-Nady, O., & Khudeir, A. (1984). Tectonic evolution of the basement complex in the Central Eastern Desert of Egypt. Geologische Rundschau, 73(3), 1019-1036.

Ferguson, C. B., Duebendorfer, E. M., & Chamberlain, K. R. (2004). Synkinematic intrusion of the 1.4-Ga Boriana Canyon pluton, northwestern Arizona: Implications for ca. 1.4-Ga regional strain in the western United States. The Journal of Geology, 112(2), 165-183.

Ferré, E. C., Bordarier, C., & Marsh, J. S. (2002). Magma flow inferred from AMS fabrics in a layered mafic sill, Insizwa, South Africa. Tectonophysics, 354(1-2), 1-23.

Ferré, E. C., Galland, O., Montanari, D., & Kalakay, T. J. (2012). Granite magma migration and emplacement along thrusts. International Journal of Earth Sciences, 101(7), 1673-1688.

Fowler, A. R., & El Kalioubi, B. (2004). Gravitational collapse origin of shear zones, foliations and linear structures in the Neoproterozoic cover nappes, Eastern Desert, Egypt. Journal of African Earth Sciences, 38(1), 23-40.

Fowler, T. J., & Osman, A. F. (2001). Gneiss-cored interference dome associated with two phases of late Pan-African thrusting in the central Eastern Desert, Egypt. Precambrian Research, 108(1-2), 17-43.

Fritz, H. & Puhl, J. (1996). Granitoid emplacement in a shear-extensional setting: A semiquantitative approach from physical parameters (Eastern Desert, Egypt). Zentralblatt Geologie Paläontologie, 257– 276.

Fritz, H., & Messner, M. (1999). Intramontane basin formation during oblique convergence in the Eastern Desert of Egypt: magmatically versus tectonically induced subsidence. Tectonophysics, 315(1-4), 145-162.

Fritz, H., Dallmeyer, D. R., Wallbrecher, E., Loizenbauer, J., Hoinkes, G., Neumayr, P., & Khudeir, A. A. (2002). Neoproterozoic tectonothermal evolution of the Central Eastern Desert, Egypt: a slow velocity tectonic process of core complex exhumation. Journal of African Earth Sciences, 34(3-4), 137-155.

Fritz, H., Loizenbauer, J., & Wallbrecher, E. (2014). Magmatic and solid state structures of the Abu Ziran pluton: deciphering transition from thrusting to extension in the Eastern Desert of Egypt. Journal of African Earth Sciences, 99, 122-135.

Fritz, H., Wallbrecher, E., Khudeir, A. A., El Ela, F. A., & Dallmeyer, D. R. (1996). Formation of Neoproterozoic metamorphic complex during oblique convergence (Eastern Desert, Egypt). Journal of African Earth Sciences, 23(3), 311-329.

Galland, O., Cobbold, P. R., de Bremond d'Ars, J., & Hallot, E. (2007). Rise and emplacement of magma during horizontal shortening of the brittle crust: Insights from experimental modeling. Journal of Geophysical Research: Solid Earth, 112(B6).

Galland, O., Cobbold, P. R., Hallot, E., & de Bremond d'Ars, J. (2008). Magma-controlled tectonics in compressional settings; insights from geological examples and experimental modelling. Bollettino della Societa Geologica Italiana, 127(2), 205-208.

Galland, O., Cobbold, P. R., Hallot, E., de Bremond d'Ars, J., & Delavaud, G. (2006). Use of vegetable oil and silica powder for scale modelling of magmatic intrusion in a deforming brittle crust. Earth and Planetary Science Letters, 243(3-4), 786-804.

Galland, O., Planke, S., Neumann, E. R., & Malthe-Sørenssen, A. (2009). Experimental modelling of shallow magma emplacement: Application to saucer-shaped intrusions. Earth and Planetary Science Letters, 277(3-4), 373-383.

Galland, O., Spacapan, J.B., Rabbel, O., Mair, K., Soto, F.G., Eiken, T., Schiuma, M. and Leanza, H.A.J.J.o.S.G. (2019). Structure, emplacement mechanism and magma-flow significance of igneous fingers–Implications for sill emplacement in sedimentary basins. 124: 120-135.

Gerya, T. V., & Burg, J. P. (2007). Intrusion of ultramafic magmatic bodies into the continental crust: numerical simulation. Physics of the Earth and Planetary Interiors, 160(2), 124-142.

Greiling, R. O., Abdeen, M. M., Dardir, A. A., El Akhal, H., El Ramly, M. F., El Din Kamal, G. M., Ali Farrag Osman, A. A. Rashwan, A. H. N. Rice & Sadek, M. F. (1994). A structural synthesis of the Proterozoic Arabian-Nubian Shield in Egypt. Geologische Rundschau, 83(3), 484-501.

Habib, M. E., Ahmed, A. A., & El Nady, O. M. (1985a). Tectonic evolution of the Meatiq infrastructure, central Eastern Desert, Egypt. Tectonics, 4(7), 613-627.

Habib, M. E., Ahmed, A. A., & El Nady, O. M. (1985b). Two orogenies in the Meatiq area of the central Eastern Desert, Egypt. Precambrian Research, 30(2), 83-111.

Hamdy, M. M., Abd El-Wahed, M. A., El Dien, H. G., & Morishita, T. (2017). Garnet hornblendite in the Meatiq Core Complex, Central Eastern Desert of Egypt: implications for crustal thickening preceding the∼ 600 Ma extensional regime in the Arabian-Nubian Shield. Precambrian Research, 298, 593-614.

Hamilton, W. B. (1994). Subduction systems and magmatism. In: Smellie JL (ed) Volcanism associated with extension at consuming plate margins. Special Publication, vol 81. Geological Society, London, pp 3–28.

Hamimi, Z., & Abd El-Wahed, M. A. (2020). Suture (s) and major shear zones in the Neoproterozoic basement of Egypt. The Geology of Egypt, 153-189.

Hassan, S. M., Taha, M. M., El Kazzaz, Y. & Mohammad, A. T. (2017). Late Neoproterozoic basement rocks of Meatiq area, Central Eastern Desert, Egypt: Petrography and remote sensing characterizations. Journal of African Earth Sciences, 131, 14-31.

Hogan, J. P., Price, J. D., & Gilbert, M. C. (1998). Magma traps and driving pressure: consequences for pluton shape and emplacement in an extensional regime. Journal of Structural Geology, 20(9-10), 1155-1168.

Horsman, E., Morgan, S., de Saint-Blanquat, M., Habert, G., Nugent, A., Hunter, R. A., & Tikoff, B. (2009). Emplacement and assembly of shallow intrusions from multiple magma pulses, Henry Mountains, Utah. Earth and Environmental Science Transactions of the Royal Society of Edinburgh, 100(1-2), 117-132.

Hutton, D. H. (1982). A tectonic model for the emplacement of the Main Donegal Granite, NW Ireland. Journal of the Geological Society, 139(5), 615-631.

Hutton, D. H. (1988). Granite emplacement mechanisms and tectonic controls: inferences from deformation studies. Earth and Environmental Science Transactions of the Royal Society of Edinburgh, 79(2-3), 245-255.

Hutton, D. H. (1992). Granite sheeted complexes: evidence for the dyking ascent mechanism. Earth and Environmental Science Transactions of the Royal Society of Edinburgh, 83(1-2), 377-382.

Hutton, D. H. (1996). The space problem in the emplacement of granite. Episodes Journal of International Geoscience, 19(4), 114-119.

Hutton, D. H. W., & Reavy, R. J. (1992). Strike-slip tectonics and granite petrogenesis. Tectonics, 11(5), 960-967.

Hutton, D. H. W., Dempster, T. J., Brown, P. E., & Becker, S. D. (1990). A new mechanism of granite emplacement: intrusion in active extensional shear zones. Nature, 343(6257), 452-455.

Hutton, D. H., & Ingram, G. M. (1992). The Great Tonalite Sill of southeastern Alaska and British Columbia: emplacement into an active contractional high angle reverse shear zone. Earth and Environmental Science Transactions of The Royal Society of Edinburgh, 83(1-2), 383-386.

Ingram, G. M., & Hutton, D. H. (1994). The Great Tonalite Sill: Emplacement into a contractional shear zone and implications for Late Cretaceous to early Eocene tectonics in southeastern Alaska and British Columbia. Geological Society of America Bulletin, 106(5), 715-728.

Johnson, P. R., Andresen, A., Collins, A. S., Fowler, A. R., Fritz, H., Ghebreab, W., Kusky, T. & Stern, R. J. (2011). Late Cryogenian–Ediacaran history of the Arabian–Nubian Shield: a review of depositional, plutonic, structural, and tectonic events in the closing stages of the northern East African Orogen. Journal of African Earth Sciences, 61(3), 167-232.

Kalakay, T. J., John, B. E., & Lageson, D. R. (2001). Fault-controlled pluton emplacement in the Sevier fold-and-thrust belt of southwest Montana, USA. Journal of Structural Geology, 23(6-7), 1151-1165.

Kamal El Din, G.M. 1(993). Geochemistry and Tectonic Significance of the Pan-African El Sibai Window, Central Eastern Desert, Egypt. Unpubl. PhD Thesis. Forschungzentrum Julich GmbH, vol. 19, p. 154.

Karlstrom, K. E., Miller, C. F., Kingsbury, J. A., & Wooden, J. L. (1993). Pluton emplacement along an active ductile thrust zone, Piute Mountains, southeastern California: Interaction between deformational and solidification processes. Geological Society of America Bulletin, 105(2), 213-230.

Khudeir, A. A., Abu El-Rus, M. A., El-Gaby, S., El-Nady, O., & Bishara, W. W. (2008). Sr–Nd isotopes and geochemistry of the infrastructural rocks in the Meatiq and Hafafit core complexes, Eastern Desert, Egypt: Evidence for involvement of pre-Neoproterozoic crust in the growth of Arabian–Nubian Shield. Island Arc, 17(1), 90-108.

Kiyokawa, S., Suzuki, T., El-Dokouny, H. A., Dawoud, M., & Abuelhasan, M. M. (2020b). Stratigraphy, petrology, and geochemistry of a neoproterozoic banded iron sequence in the El-Dabbah Group, central Eastern Desert, Egypt. Journal of African Earth Sciences, 168, 103805.

Kiyokawa, S., Suzuki, T., Horie, K., Takehara, M., El-Dokouny, H. A., Dawoud, M., & Abuelhasan, M. M. (2020a). Tectonic and sedimentary history of the neoproterozoic metavolcanic–volcaniclastic rocks of the El-Dabbah Group, Central Eastern Desert, Egypt. Journal of African Earth Sciences, 165, 103807.

Köpping, J. (2022): From planes to pipes: The emplacement of elongate intrusions in shallow magma plumbing systems. Monash University. PhD Thesis. https://doi.org/10.26180/193651-34.v2

Köpping, J., Magee, C., Cruden, A. R., Jackson, C. A. L., & Norcliffe, J. R. (2022). The building blocks of igneous sheet intrusions: Insights from 3-D seismic reflection data. Geosphere, 18(1), 156-182.

Loizenbauer, J., Wallbrecher, E., Fritz, H., Neumayr, P., Khudeir, A. A., & Kloetzli, U. (2001). Structural geology, single zircon ages and fluid inclusion studies of the Meatiq metamorphic core complex: implications for Neoproterozoic tectonics in the Eastern Desert of Egypt. Precambrian Research, 110(1-4), 357-383.

Lundmark, A. M., Andresen, A., Hassan, M. A., Augland, L. E., & Boghdady, G. Y. (2012). Repeated magmatic pulses in the East African Orogen in the Eastern Desert, Egypt: an old idea supported by new evidence. Gondwana Research, 22(1), 227-237.

Magee, C., Muirhead, J., Schofield, N., Walker, R. J., Galland, O., Holford, S., Spacapan, J., Jackson, C.A. & McCarthy, W. (2019). Structural signatures of igneous sheet intrusion propagation. Journal of Structural Geology, 125, 148-154.

Magee, C., Muirhead, J.D., Karvelas, A., Holford, S.P., Jackson, C.A., Bastow, I.D., Schofield, N., Stevenson, C.T., McLean, C. and McCarthy, W., (2016). Lateral magma flow in mafic sill complexes. Geosphere: GES01256. 01251

McCaffrey, K. J. (1989). The emplacement and deformation of granitic rocks in a transpressional shear zone: The Ox Mountains Igneous Complex (Doctoral dissertation, Durham University).

McCaffrey, K. J. W. (1992). Igneous emplacement in a transpressive shear zone: Ox Mountains igneous complex. Journal of the Geological Society, 149(2), 221-235.

Michel, J., Baumgartner, L., Putlitz, B., Schaltegger, U., & Ovtcharova, M. (2008). Incremental growth of the Patagonian Torres del Paine laccolith over 90 ky. Geology, 36(6), 459-462.

Mohamed, Haroun & Abdel Ghani, M. (2000). Contribution to the Geochemistry and Petrogenesis of Abu Ziran Older Granitoids, central Eastern Desert, Egypt. Faculty of Science Bulletin. 29 (1-F). 55 - 68.

Mohammad, A. T., El Kazzaz, Y. A., Hassan, S. M., & Taha, M. M. (2020). Neoproterozoic tectonic evolution and exhumation history of transpressional shear zones in the East African orogen: implications from kinematic analysis of Meatiq area, Central Eastern Desert of Egypt. International Journal of Earth Sciences, 109(1), 253-279.

Muirhead, J. D., Kattenhorn, S. A., & Le Corvec, N. (2015). Varying styles of magmatic strain accommodation across the East A frican R ift. Geochemistry, Geophysics, Geosystems, 16(8), 2.

Musumeci, G., Mazzarini, F., Corti, G., Barsella, M., & Montanari, D. (2005). Magma emplacement in a thrust ramp anticline: The Gavorrano Granite (northern Apennines, Italy). Tectonics, 24(6).

Myers, J. S. (1975). Cauldron subsidence and fluidization: mechanisms of intrusion of the Coastal Batholith of Peru into its own volcanic ejecta. Geological Society of America Bulletin, 86(9), 1209-1220.

Naibert, T. J., Geissman, J. W., & Heizler, M. T. (2010). Magnetic fabric, paleomagnetic, and 40Ar/39Ar geochronologic data bearing on the emplacement of the Late Cretaceous Philipsburg Batholith, SW Montana fold-and-thrust belt. Lithosphere, 2(5), 303-327.

Neumayr, P., Hoinkes, G., Puhl, J., Mogessie, A., & Khudeir, A. A. (1998). The Meatiq dome (Eastern Desert, Egypt) a Precambrian metamorphic core complex: petrological and geological evidence. Journal of Metamorphic Geology, 16(2), 259-279.

Neumayr, P., Mogessie, A., Hoinkes, G., & Puhl, J. (1996). Geological setting of the Meatiq metamorphic core complex in the Eastern Desert of Egypt based on amphibolite geochemistry. Journal of African Earth Sciences, 23(3), 331-345.

Neves, S. P., & Mariano, G. (1999). Assessing the tectonic significance of a large-scale transcurrent shear zone system: the Pernambuco lineament, northeastern Brazil. Journal of Structural Geology, 21(10), 1369-1383.

Neves, S. P., & Vauchez, A. (1995). Magma emplacement and shear zone nucleation and development in northeast Brazil (Fazenda Nova and Pernambuco shear zones; State of Pernambuco). Journal of South American Earth Sciences, 8(3-4), 289-298.

Neves, S. P., Vauchez, A., & Archanjo, C. J. (1996). Shear zone-controlled magma emplacement or magma-assisted nucleation of shear zones? Insights from northeast Brazil. Tectonophysics, 262(1-4), 349-364.

Nyman, M. W., & Karlstrom, K. E. (1997). Pluton emplacement processes and tectonic setting of the 1.42 Ga Signal batholith, SW USA: important role of crustal anisotropy during regional shortening. Precambrian Research, 82(3-4), 237-263.

Papeschi, S., Mazzarini, F., Musumeci, G., & Cruden, A.R. (2022). Emplacement of a felsic dyke swarm during progressive heterogeneous deformation, Eastern Elba Dyke Complex (Island of Elba, Italy), Journal of Structural Geology. doi: https://doi.org/10.1016/j.jsg.2022.104600.

Paterson, S. R. (2005). Close spatial relationship between plutons and shear zones: Comment and Reply: COMMENT. Geology, 33 (1): e72.

Paterson, S. R., & Schmidt, K. L. (1999). Is there a close spatial relationship between faults and plutons?. Journal of Structural Geology, 21(8-9), 1131-1142.

Paterson, S. R., Vernon, R. H., & Tobisch, O. T. (1989). A review of criteria for the identification of magmatic and tectonic foliations in granitoids. Journal of structural geology, 11(3), 349-363.

Petford, N., & Koenders, M. A. (1998). Granular flow and viscous fluctuations in low Bagnold number granitic magmas. Journal of the Geological Society, 155(5), 873-881.

Petford, N., Clemens, J. D., & Vigneresse, J. L. (1997). Application of information theory to the formation of granitic rocks. In Granite: From segregation of melt to emplacement fabrics (pp. 3-10). Springer, Dordrecht.

Petford, N., Cruden, A. R., McCaffrey, K. J. W., & Vigneresse, J. L. (2000). Granite magma formation, transport and emplacement in the Earth's crust. Nature, 408(6813), 669-673.

Pitcher, W. S. (1979). The nature, ascent and emplacement of granitic magmas. Journal of the Geological Society, 136(6), 627-662.

Pitcher, W. S., & Bussell, M. A. (1977). Structural control of batholithic emplacement in Peru: a review. Journal of the Geological Society, 133(3), 249-255.

Ries, A. C., Shackleton, R. M., Graham, R. H., & Fitches, W. R. (1983). Pan-African structures, ophiolites and mélange in the Eastem Desert of Egypt: a traverse at 26 N. Journal of the Geological Society, 140(1), 75-95.

Roman-Berdiel, T., Gapais, D., & Brun, J. P. (1995). Analogue models of laccolith formation. Journal of Structural Geology, 17(9), 1337-1346.

Roman-Berdiel, T., Gapais, D., & Brun, J. P. (1997). Granite intrusion along strike-slip zones in experiment and nature. American Journal of Science, 297(6), 651-678.

Rosenberg, C. L. (2004). Shear zones and magma ascent: a model based on a review of the Tertiary magmatism in the Alps. Tectonics, 23(3).

Rosenberg, C. L., Berger, A., & Schmid, S. M. (1995). Observations from the floor of a granitoid pluton: Inferences on the driving force of final emplacement. Geology, 23(5), 443-446.

Schmidt, K. L. & Paterson, S. R. (2000). Analyses fail to find coupling between deformation and magmatism. Eos 81(197):202–203.

Schofield, N.J., Brown, D.J., Magee, C. and Stevenson, C.T., 2012. Sill morphology and comparison of brittle and non-brittle emplacement mechanisms. Journal of the Geological Society, 169(2): 127-141.

Searle, M. P. (1999). Emplacement of Himalayan leucogranites by magma injection along giant sill complexes: examples from the Cho Oyu, Gyachung Kang and Everest leucogranites (Nepal Himalaya). Journal of Asian Earth Sciences, 17(5-6), 773-783.

Shalaby, A. (2010). The northern dome of Wadi Hafafit culmination, Eastern Desert, Egypt: structural setting in tectonic framework of a scissor-like wrench corridor. Journal of African Earth Sciences, 57(3), 227-241.

Shalaby, A., Stüwe, K., Fritz, H., & Makroum, F. (2006). The El Mayah molasse basin in the Eastern Desert of Egypt. Journal of African Earth Sciences, 45(1), 1-15.

Shalaby, A., Stüwe, K., Makroum, F., Fritz, H., Kebede, T., & Klötzli, U. (2005). The Wadi Mubarak belt, Eastern Desert of Egypt: a Neoproterozoic conjugate shear system in the Arabian–Nubian Shield. Precambrian Research, 136(1), 27-50.

Sharib, A. S. A., Maurice, A. E., Abd El-Rahman, Y. M., Sanislav, I. V., Schulz, B., & Bakhit, B. R. (2019). Neoproterozoic arc sedimentation, metamorphism and collision: Evidence from the northern tip of the Arabian-Nubian Shield and implication for the terminal collision between East and West Gondwana. Gondwana Research, 66, 13-42.

Shimura, T. (1992). Intrusion of granitic magma and uplift tectonics of the Hidaka metamorphic belt, Hokkaido. Chishitsugaku Zasshi, 98(1), 1-20.

Sibson, R. H. (2003) Brittle-failure controls on maximum sustainable overpressure in different tectonic regimes. Am Assoc Petroleum Geol. Bull 87(6), 901–908.

Spanner, B. G., & Kruhl, J. H. (2002). Syntectonic granites in thrust and strike–slip regimes: the history of the Carmo and Cindacta plutons (southeastern Brazil). Journal of South American Earth Sciences, 15(4), 431-444.

Stern, R. J. (1985). The Najd fault system, Saudi Arabia and Egypt: A late Precambrian rift-related transform system?. Tectonics, 4(5), 497-511.

Stern, R. J. (1994). Arc assembly and continental collision in the Neoproterozoic East African Orogen: implications for the consolidation of Gondwanaland. Annual Review of Earth and Planetary Sciences, 22(1), 319-351.

Stern, R. J. (2018). Neoproterozoic formation and evolution of Eastern Desert continental crust–The importance of the infrastructure-superstructure transition. Journal of African Earth Sciences, 146, 15-27.

Stern, R. J., & Ali, K. (2020). Crustal evolution of the Egyptian Precambrian rocks. In The Geology of Egypt (pp. 131-151). Springer, Cham.

Stern, R.J., and Hedge, C.E. (1985). Geochronologic and isotopic constraints on late Precambrian crustal evolution in the Eastern Desert of Egypt: American Journal of Science, v. 285, p. 97-127.

Sturchio, N. C. (1983). Geology, petrology and geochronology of the metamorphic rocks of Meatiq Dome, Central Eastern Desert, Egypt. Washington University in St. Louis. PhD Thesis.

Sturchio, N. C., Sultan, M., & Batiza, R. (1983). Geology and origin of Meatiq Dome, Egypt: A Precambrian metamorphic core complex?. Geology, 11(2), 72-76.

Sultan, M. (1984). Geology, petrology and geochemistry of a younger granite pluton, Central eastern Desert of Egypt: Importance of mixing. Washington University in St. Louis. PhD Thesis.

Sultan, M., Arvidson, R. E., Duncan, I. J., Stern, R. J., & El Kaliouby, B. (1988). Extension of the Najd shear system from Saudi Arabia to the central Eastern Desert of Egypt based on integrated field and Landsat observations. Tectonics, 7(6), 1291-1306.

Tobisch, O. T., & Paterson, S. R. (1990). The Yarra granite: an intradeformational pluton associated with ductile thrusting, Lachlan Fold Belt, southeastern Australia. Geological Society of America Bulletin, 102(6), 693-703.

Toyoshima, T., Komatsu, M., & Shimura, T. (1994). Tectonic evolution of lower crustal rocks in an exposed magmatic arc section in the Hidaka metamorphic belt, Hokkaido, northern Japan. Island Arc, 3(3), 182-198.

Vigneresse, J. L. (1995). Control of granite emplacement by regional deformation. Tectonophysics, 249(3-4), 173-186.

Vigneresse, J. L., & Tikoff, B. (1999). Strain partitioning during partial melting and crystallizing felsic magmas. Tectonophysics, 312(2-4), 117-132.

Vigneresse, J. L., Tikoff, B., & Améglio, L. (1999). Modification of the regional stress field by magma intrusion and formation of tabular granitic plutons. Tectonophysics, 302(3-4), 203-224.

Wadge, G., & Cross, A. (1988). Quantitative methods for detecting aligned points: An application to the volcanic vents of the Michoacan-Guanajuato volcanic field, Mexico. Geology, 16(9), 815-818.

Walsh, J., Bailey W., Childs C., Nicol A.& Bonson C. (2003). Formation of segmented normal faults: a 3-D perspective J. Struct. Geol., 25, 1251-1262.

Watanabe, T., Koyaguchi, T., & Seno, T. (1999). Tectonic stress controls on ascent and emplacement of magmas. Journal of Volcanology and Geothermal Research, 91(1), 65-78.

Watanabe, T., Koyaguchi, T., & Seno, T. (1999). Tectonic stress controls on ascent and emplacement of magmas. Journal of Volcanology and Geothermal Research, 91(1), 65-78.

Weinberg, R. F., Sial, A. N., & Mariano, G. (2004). Close spatial relationship between plutons and shear zones. Geology, 32(5), 377-380.

Weinberg, R. F., Sial, A. N., & Mariano, G. (2005). Close spatial relationship between plutons and shear zones: Comment and Reply: REPLY. Geology, 33 (1): e74.

Žák, J., Verner, K., Sláma, J., Kachlík, V., & Chlupáčová, M. (2013). Multistage magma emplacement and progressive strain accumulation in the shallow-level Krkonoše-Jizera plutonic complex, Bohemian Massif. Tectonics, 32(5), 1493-1512.

Zoheir, B. A., Creaser, R. A., & Lehmann, B. (2015). Re-Os geochronology of gold mineralization in the Fawakhir area, Eastern Desert, Egypt. International Geology Review, 57(11-12), 1418-1432.

Zoheir, B., Zeh, A., El-Bialy, M., Ragab, A., Deshesh, F., & Steele-MacInnis, M. (2021). Hybrid granite magmatism during orogenic collapse in the Eastern Desert of Egypt: Inferences from whole-rock geochemistry and zircon U–Pb–Hf isotopes. Precambrian Research, 354, 106044.

Captions

Fig.1. (a) Simplified map showing the northern parts of Arabian and Nubian Shields, and the location of Fig. b. (b) simplified geological map of the CED, the rectangle indicates the location of Fig. c, (M: Meatiq dome, U: Um Had dome, Sh: Sl Shalul dome, S: El Sibai dome, HSZ: Hamrawin Shear Zone, EMSZ: East Meatiq Shear Zone, ASZ: Atalla Shear Zone). (c) geological map of Meatiq dome, the ages of granite intrusions are based on the work of Andresen et al., (2009).

Fig.2. Outcrop-scale structures of MSZ. (a), (b) sigmoidal-shaped boudins in quartz with a sigma-type pressure shadow indicating top-to-NW tectonic transport. (c) asymmetrical lens-shaped quartz boudin in mylonitic schist reveal top-to-NW sense of movement. (d) symmetrical bench and swell structure indicating NW-SE stretching. (e) recumbent chevron fold in quartzo-feldspathic schists. (f) recumbent chevron fold in quartzo-feldspathic schists displaying transposed foliation related to intense shearing. (g) asymmetrical folds indicating a top-to-NW sense of shearing. (h) recumbent, similar folds in quartzo-feldspathic schists.

Fig.3. Microscopic features of MSZ mylonites. (a) pronounced foliation marked by aligned muscovite crystals. (b) elliptical to irregular-shaped garnet crystal with highly curved quartz inclusion trails marking an s-shaped internal foliation which implies a syn-tectonic growth. (c) Post-tectonic garnet (grt) displays euhedral crystal cross-cutting foliated minerals; biotite (bt), quartz and plagioclase. (d) sigmoidal recrystallized quartz porphyroclast with sigma-type pressure shadows indicating top-to-NW sense of shear. (e), S-C fabric in biotite-hornblende schist indicating top-to-NW sense of shear. (f) asymmetrical intrafolial fold in quartz ribbon indicating top-to-NW sense of shear.

Fig.4. Geological Map of Abu Ziran Pluton in the western part of Meatiq dome.

Fig.5. Outcrop- scale magmatic and tectonic structures of Abu Ziran pluton. (a) mafic layering and schlieren in the southern outcrop. (b) alternating felsic and mafic banding of magmatic origin. (c) stretched mafic enclaves in mylonitic granite, dissected by brittle thrust fault. (d) stretched mafic enclaves parallel to mylonitic fabric, with a dyke of sheared pegmatitic tonalite. (e) close view of the sheared dyke. (f) thrust duplex in Abu Ziran pluton, verging to NW, and crosscut all ductile fabrics. (g) close view of the thrust fault plane with clear slickenlines plunging SW.

Fig.6. Microscopic features of Abu Ziran granites. (a) magmatic zoning in euhedral plagioclase crystal. (b) highly altered plagioclase crystal and coarse-grained quartz crystals with highly serrated boundaries indicating GBM recrystallization. (c) quartz-feldspar intergrowth possibly

related to the metasomatic effect of post-tectonic alkali granites. (d) euhedral plagioclase phenocryst with evidences of dynamic crystallization on rims. (e), (f) well-developed C-S fabric marked by aligned plagioclase porphyroclasts, mica aggregates and quartz ribbons, and indicating top-to-NW shear sense. (g) typical ductile solid-state fabric with sigmoidal-shape porphyroclast of plagioclase indicating top-to-NW shear sense. (h) size grain reduction in quartz aggregates due to SGR dynamic recrystallization. (i) weakly-developed myrmekitic texture in plagioclase porphyroclasts. (j) schematic diagram summarizing the spectrum of microstructures documented from Abu Ziran pluton.

Fig.7. Structural analysis of domain A. (a) High-resolution Satellite image and geological map of domain A, the white outline marks the boundaries of Abu Ziran granite outcrops. (b) Geological cross section across domain A, locations of the sections indicated on the geological map in (Fig. a). (c) simplified structural sketch of domain A with stereograms of foliation and lineation measurements in the wall rocks.

Fig.8. (a) the dipping floor contact of the pluton along the rim of Abu Ziran synform. (b) 3D view of satellite image illustrating the floor contact and dipping variation associated with the synform. (c) 3D view of satellite image illustrating the tabular (sheet-shaped) geometry of Abu Ziran pluton. (d) panoramic view of Abu Ziran sheet intrusion sandwiched between mylonitic metasediments and amphibolites. (e) the contact between deformed granite and mylonites, with clear mylonitic fabric parallel to the foliation in host rocks. (f) close view of the fabrics I the granite and local gneissification. (g) intensely deformed and foliated granite sheets intruded the mylonites parallel to Abu Ziran pluton.

Fig.9. Structural analysis of domain B. (a) High-resolution Satellite image and geological map of domain b, the white outline marks the boundaries of Abu Ziran granite outcrops. (b) Geological cross section across domain b, locations of the sections indicated on the geological map in (Fig. a). (c) simplified structural sketch of domain A with stereograms of foliation 3D view of satellite image draped on DEM illustrating the floor contact of the pluton and dipping variation associated with Abu Ziran synform. (d) 3D block diagram illustrates the architecture of Abu Ziran pluton in domain B.

Fig.10. (a) exposed floor contact of Abu Ziran pluton in domain B, overlying the amphibolites parallel to tectonic fabric. (b) well-developed L-tectonites in Abu Ziran pluton along the rim of pluton. (c) Google Earth image show the intrusive relationships between Abu Ziran granite and the post-tectonic alkali granites. (d) Intrusive contacts between Abu Ziran granite and the alkali granites. (e) xenolith of Abu Ziran tonalite within alkali granite.

Fig.11. Structural analysis of domain C. (a) panoramic view of the dipping sheet-intrusion and its contacts with mylonites and ophiolitic nappes. (b) exposed floor contact of Abu Ziran pluton at domain C. (c) close view of the contact between granite and schist. (d) frequent stretched mafic enclaves in deformed granite. (e) 3D block diagram illustrates the architecture of Abu Ziran pluton in domain c with stereograms of foliation and lineation measurements in the wall rocks.

Fig.12. (a), (b) cross-sections across the different domains of Abu Ziran pluton. The location of sections is marked in Fig.4. (c) floor contact of Abu Ziran pluton. (d) 3D view of satellite image draped on DEM illustrating the tabular (sheet-shaped) geometry of Abu Ziran pluton. (e) high-resolution satellite image shows the remnants of Abu Ziran pluton on the crests of hills adjacent to domain A. (f) block diagram illustrate the 3D architecture of Abu Ziran pluton and associated folded MSZ. (g) 3D view of the cross-sections in (Figs.a, b) reveals the previous continuity of the pluton outcrops and the possible geometry and location of the eroded parts.

Fig.13. (a) Simplified structural map of Meatiq dome showing the hypothetical initial extent of Abu Ziran pluton during its emplacement time. (b) cross-sections across the pluton illustrate the complex present-day architecture and interpreted geometry and location of the eroded parts.

Fig.14. Mechanisms of magma intrusion in the compressional setting. (a) Dilatational flat model of Ingram and Hutton (1994). (b) magma emplacement model along steep reverse faults. (c) magma vertical escape model of Rosenberg et al., (1995). (d) Ramp-top model of Kalakay et al., (2001). (e) kinematic model for the pre-thrusting granite emplacement (after Ferre´ et al., 2012). (f) Syn-kinematic emplacement in thrust flats (after Ferre´ et al., 2012). (g) Post-kinematic emplacement in inherited thrust discontinuities (after Ferre´ et al., 2012).

Fig.15. (a) emplacement model of Abu Ziran granite as a sheet-shaped intrusion along the contact between ophiolites and mylonitic metasediments. (b) stereograms of axes of magmatic strain (Fritz et al., 2014) and axes of tectonic strain (present study). (c) schematic cross section illustrates magma emplacement mechanism and pluton growth along the MSZ. The pluton emplaced along flat segment related to crustal-scale shear zone, along the contact between ophiolites and mylonitic metasediments (d) 3D schematic diagram illustrates the geometry, extend and strain variations in Abu-Ziran pluton.

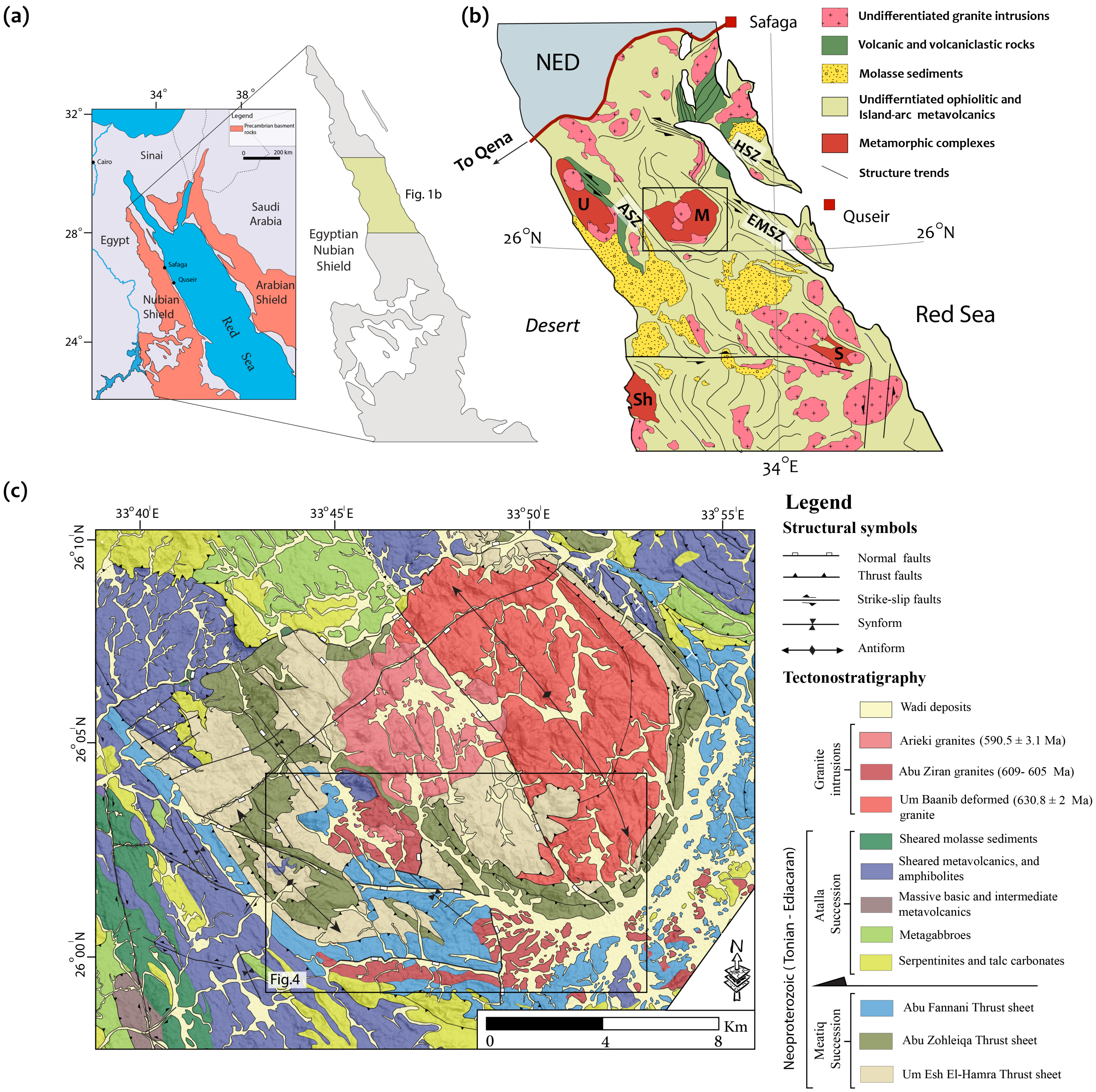

(a)
34°
38°
32°
28°
24°
Legend
Precambrian basment rocks
0
200 km
Cairo
Sinai
Egypt
Saudi Arabia
Safaga
Quseir
Nubian Shield
Arabian Shield
Red Sea
Fig. 1b
Egyptian Nubian Shield
(b)
NED
Safaga
To Qena
HSZ
U
ASZ
M
EMSZ
Quseir
26°N
26°N
Desert
Red Sea
S
Sh
34°E
Undifferentiated granite intrusions
Volcanic and volcaniclastic rocks
Molasse sediments
Undifferntiated ophiolitic and Island-arc metavolcanics
Metamorphic complexes
Structure trends
(c)
33°40'E
33°45'E
33°50'E
33°55'E
26°10'N
26°05'N
26°00'N
Fig.4
N
Km
0
4
8
Legend
Structural symbols
Normal faults
Thrust faults
Strike-slip faults
Synform
Antiform
Tectonostratigraphy
Wadi deposits
Granite intrusions
Arieki granites (590.5 ± 3.1 Ma)
Abu Ziran granites (609- 605 Ma)
Um Baanib deformed (630.8 ± 2 Ma) granite
Neoproterozoic (Tonian - Ediacaran)
Atalla Succession
Sheared molasse sediments
Sheared metavolcanics, and amphibolites
Massive basic and intermediate metavolcanics
Metagabbroes
Serpentinites and talc carbonates
Meatiq Succession
Abu Fannani Thrust sheet
Abu Zohleiqa Thrust sheet
Um Esh El-Hamra Thrust sheet

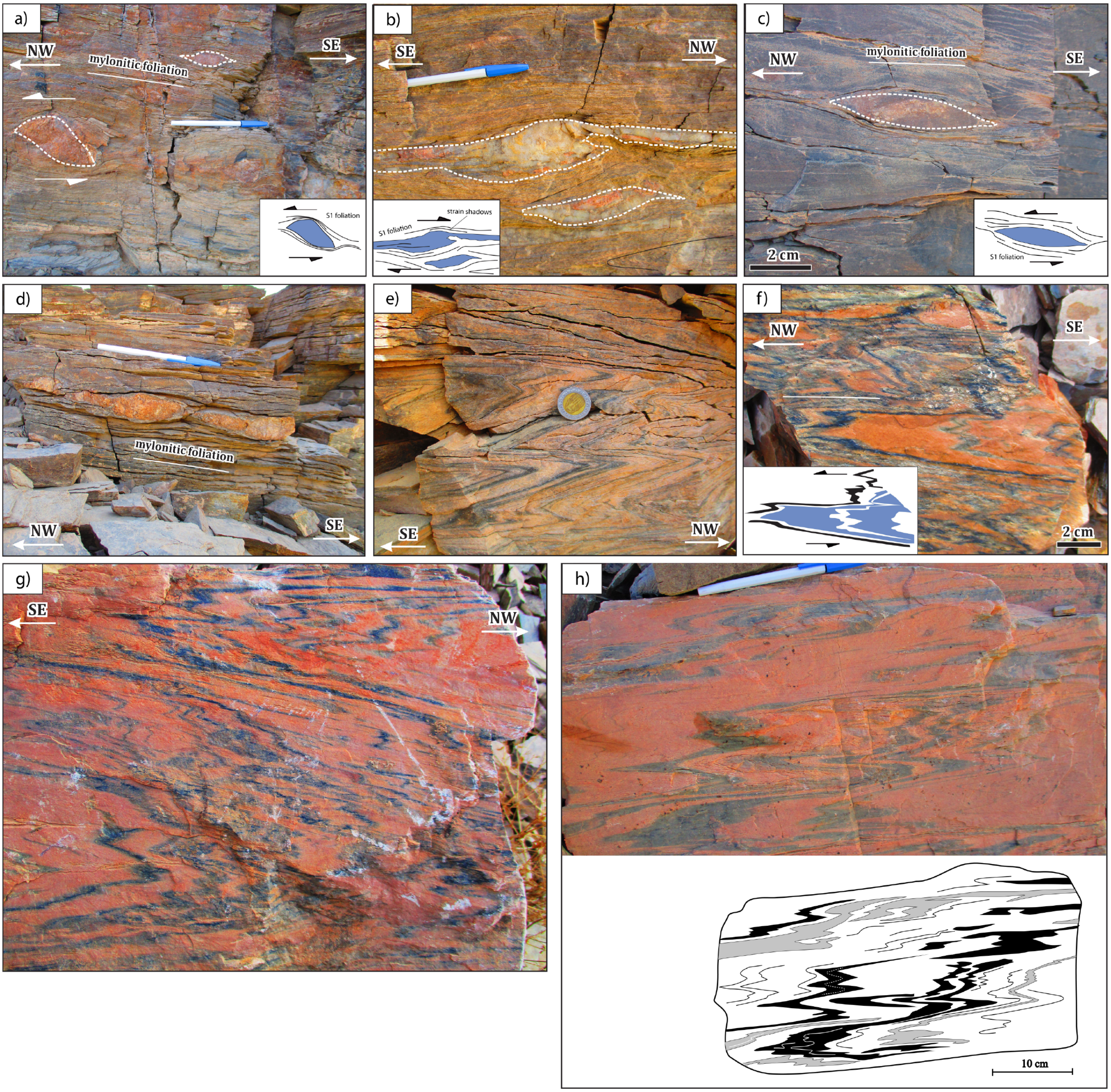

a)
NW
SE
mylonitic foliation
S1 foliation
b)
SE
NW
strain shadows
S1 foliation
c)
NW
SE
mylonitic foliation
2 cm
S1 foliation
d)
mylonitic foliation
NW
SE
e)
SE
NW
f)
NW
SE
2 cm
g)
SE
NW
h)
10 cm

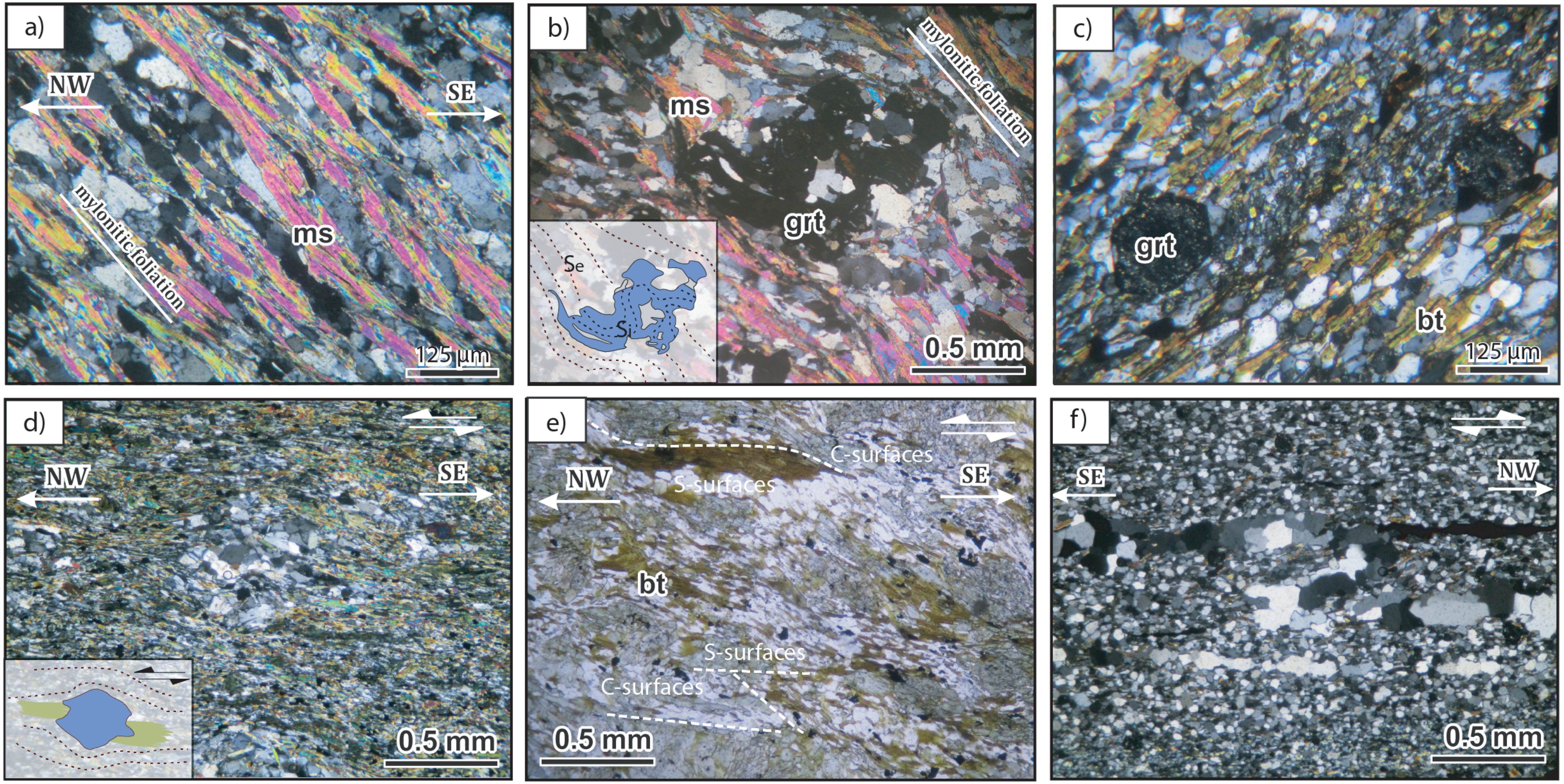

a)
NW
SE
mylonitic foliation
ms
125 µm
b)
mylonitic foliation
ms
grt
Se
Si
0.5 mm
c)
grt
bt
125 µm
d)
NW
SE
0.5 mm
e)
C-surfaces
NW
S-surfaces
SE
bt
S-surfaces
C-surfaces
0.5 mm
f)
SE
NW
0.5 mm

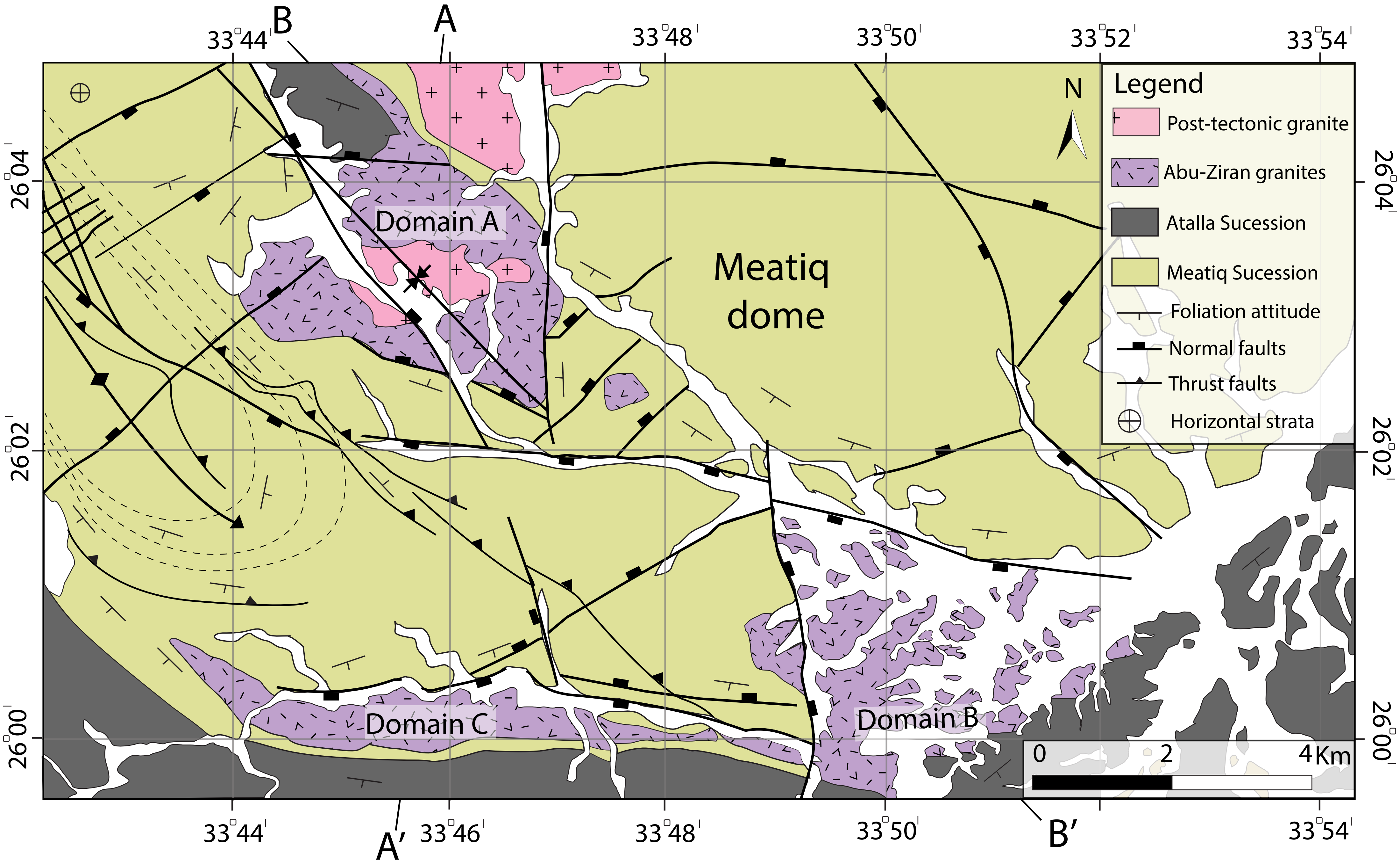
B
A
33°44'
33°48'
33°50'
33°52'
33°54'
26°04'
26°02'
26°00'
N
Legend
Post-tectonic granite
Abu-Ziran granites
Atalla Sucession
Meatiq Sucession
Foliation attitude
Normal faults
Thrust faults
Horizontal strata
Domain A
Meatiq
dome
Domain C
Domain B
0
2
4Km
A′
33°46'
B′

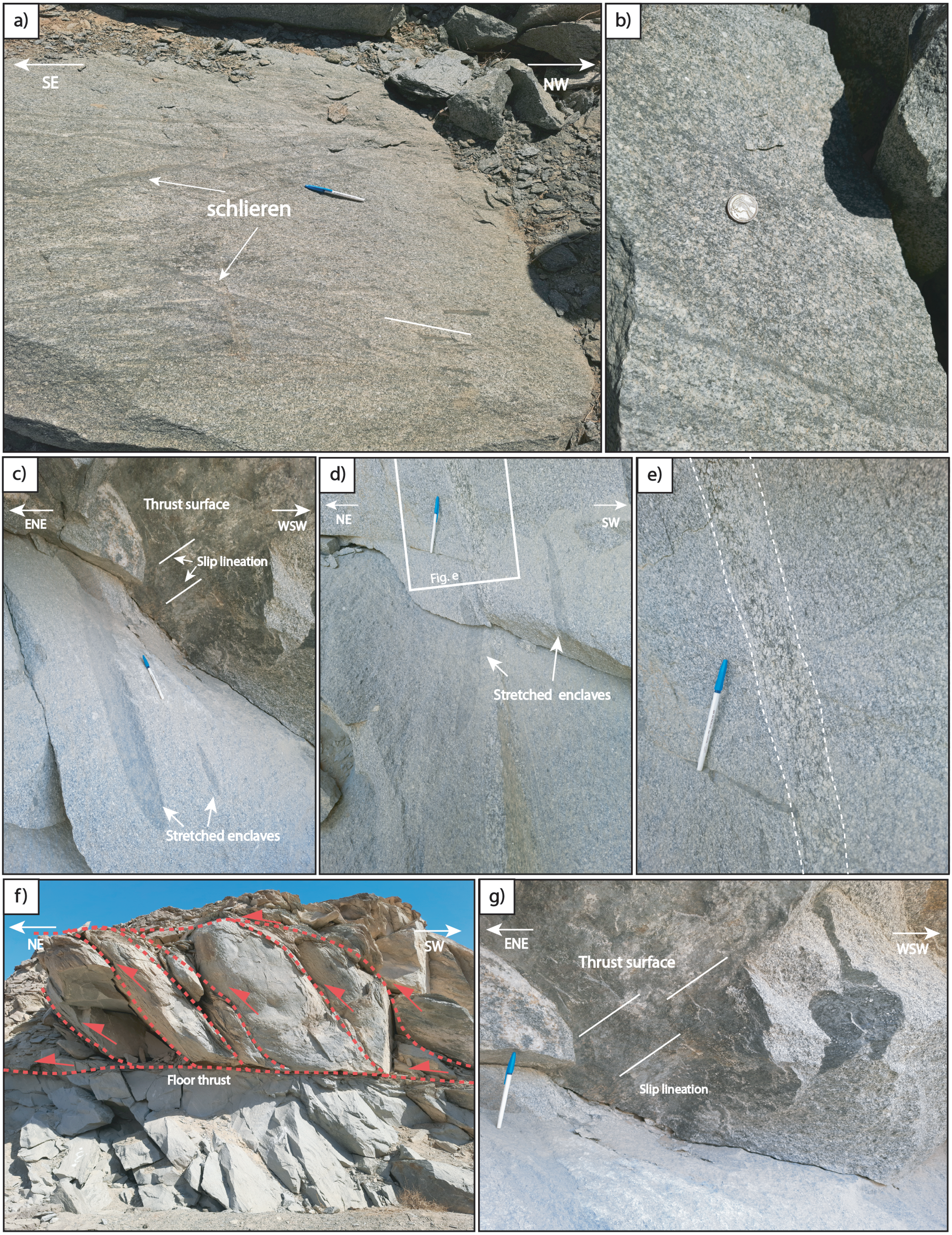
a)
SE
NW
schlieren
b)
c)
ENE
Thrust surface
WSW
Slip lineation
Stretched enclaves
d)
NE
SW
Fig. e
Stretched enclaves
e)
f)
NE
SW
Floor thrust
g)
ENE
Thrust surface
WSW
Slip lineation

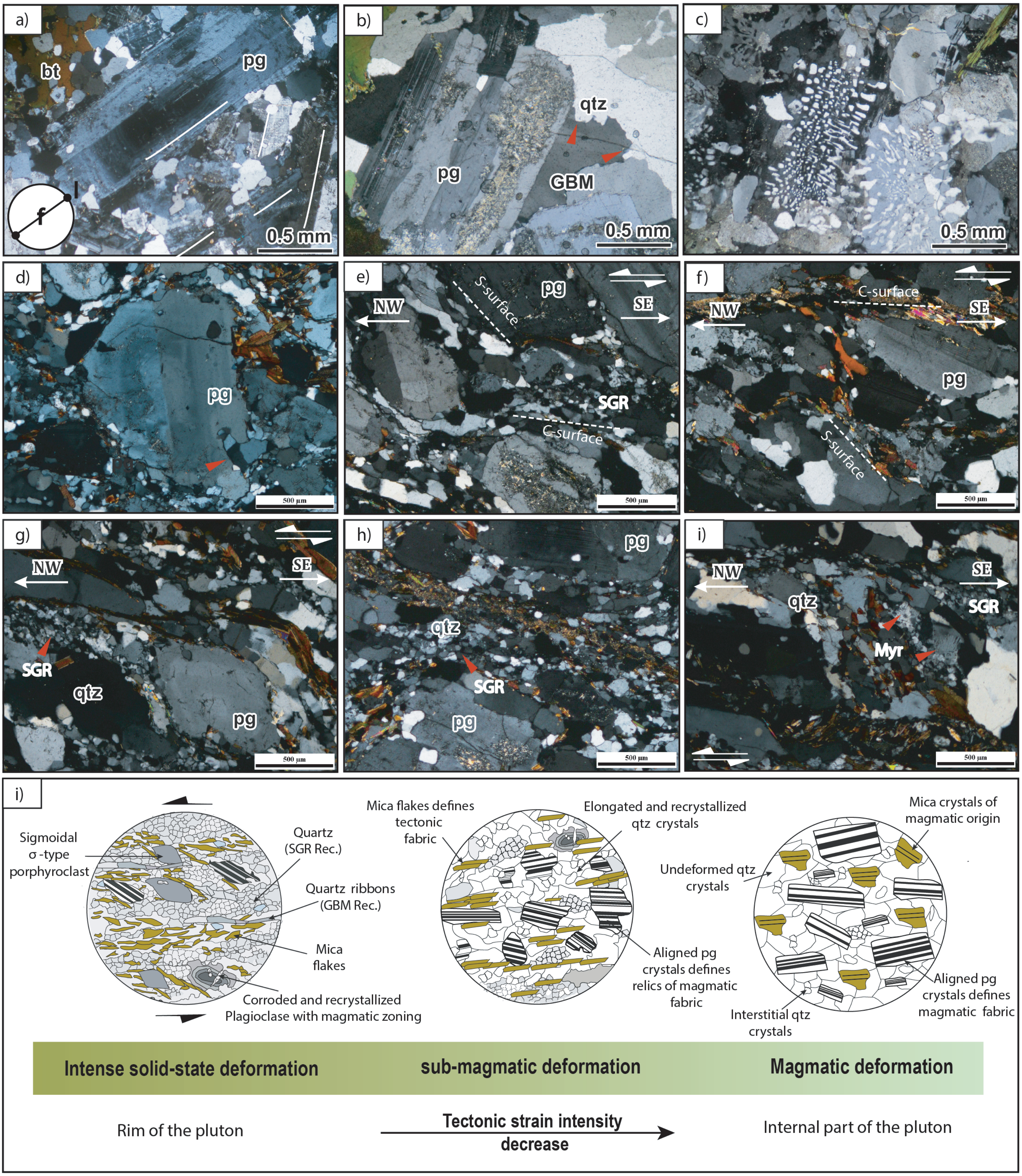

a)
bt
pg
f
l
0.5 mm
b)
qtz
pg
GBM
0.5 mm
c)
0.5 mm
d)
pg
500 µm
e)
NW
SE
S-surface
pg
SGR
C-surface
500 µm
f)
NW
SE
C-surface
pg
S-surface
500 µm
g)
NW
SE
SGR
qtz
pg
500 µm
h)
pg
qtz
SGR
pg
500 µm
i)
NW
SE
qtz
SGR
Myr
500 µm
i)
Sigmoidal σ -type porphyroclast
Quartz (SGR Rec.)
Quartz ribbons (GBM Rec.)
Mica flakes
Corroded and recrystallized Plagioclase with magmatic zoning
Mica flakes defines tectonic fabric
Elongated and recrystallized qtz crystals
Aligned pg crystals defines relics of magmatic fabric
Mica crystals of magmatic origin
Undeformed qtz crystals
Interstitial qtz crystals
Aligned pg crystals defines magmatic fabric
Intense solid-state deformation
sub-magmatic deformation
Magmatic deformation
Rim of the pluton
Tectonic strain intensity decrease
Internal part of the pluton

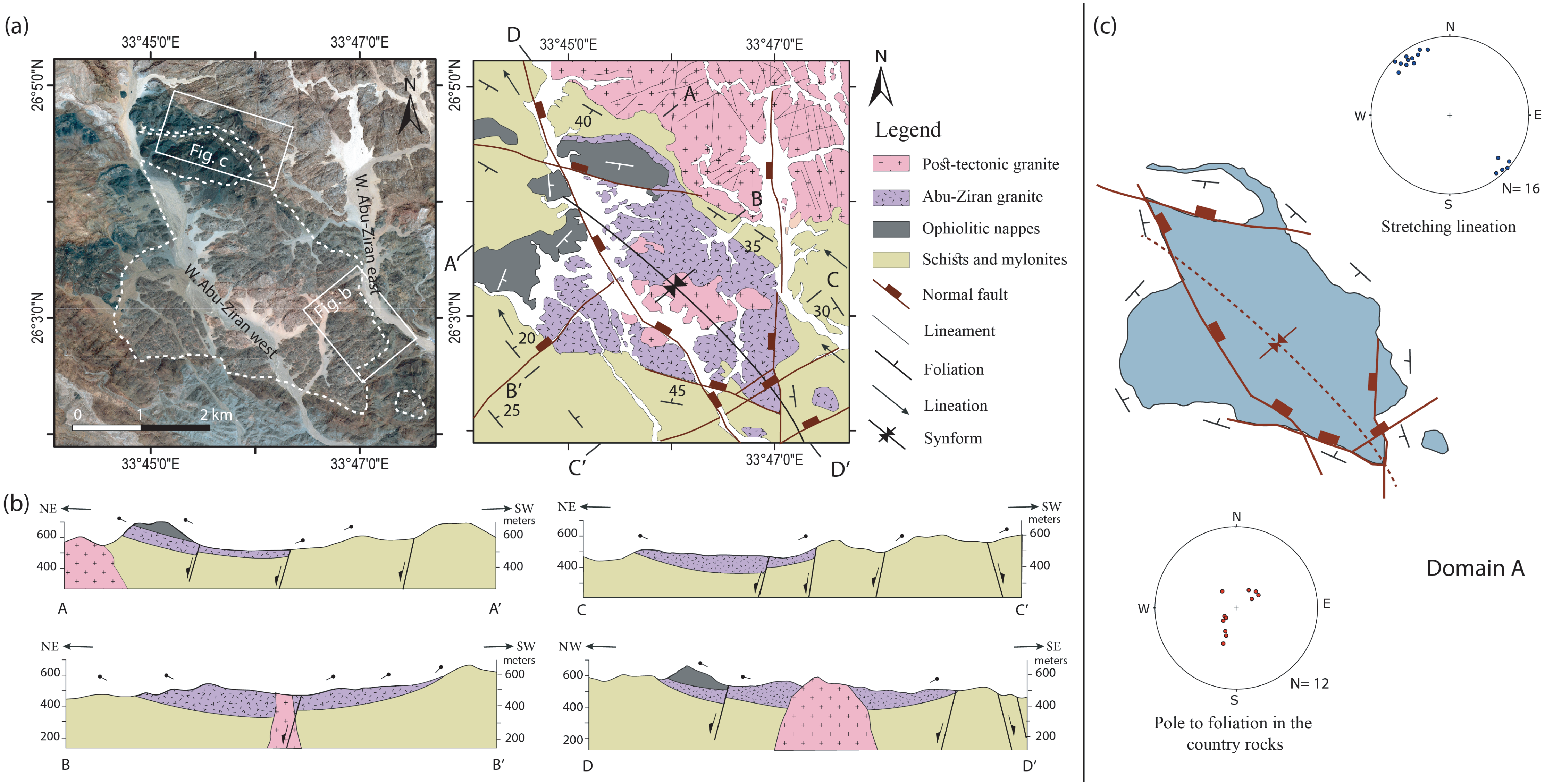
(a)
33°45'0"E
33°47'0"E
26°5'0"N
26°3'0"N
Fig. c
Fig. b
W. Abu-Ziran west
W. Abu-Ziran east
0
1
2 km
N
D
D′
A
A′
B
B′
C
C′
40
35
30
20
25
45
Legend
Post-tectonic granite
Abu-Ziran granite
Ophiolitic nappes
Schists and mylonites
Normal fault
Lineament
Foliation
Lineation
Synform
(b)
NE
SW
NW
SE
meters
600
400
200
(c)
N
S
E
W
N= 16
Stretching lineation
N= 12
Pole to foliation in the
country rocks
Domain A

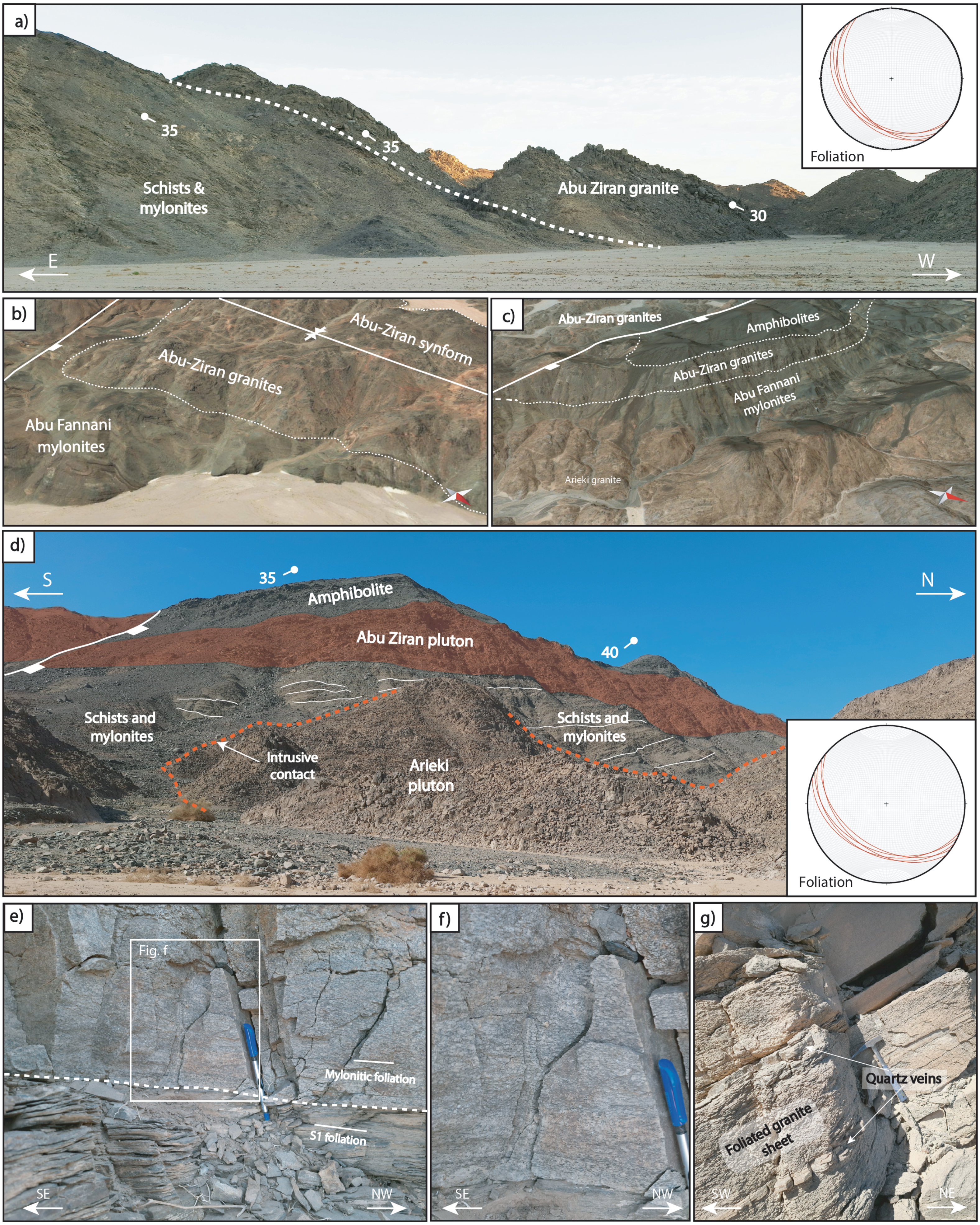
a)
Foliation
35
35
Schists &
mylonites
Abu Ziran granite
30
E
W
b)
Abu-Ziran synform
Abu-Ziran granites
Abu Fannani
mylonites
c)
Abu-Ziran granites
Amphibolites
Abu-Ziran granites
Abu Fannani
mylonites
Arieki granite
d)
S
N
35
Amphibolite
Abu Ziran pluton
40
Schists and
mylonites
Intrusive
contact
Arieki
pluton
Schists and
mylonites
Foliation
e)
Fig. f
Mylonitic foliation
S1 foliation
SE
NW
f)
SE
NW
g)
Quartz veins
Foliated granite
sheet
SW
NE

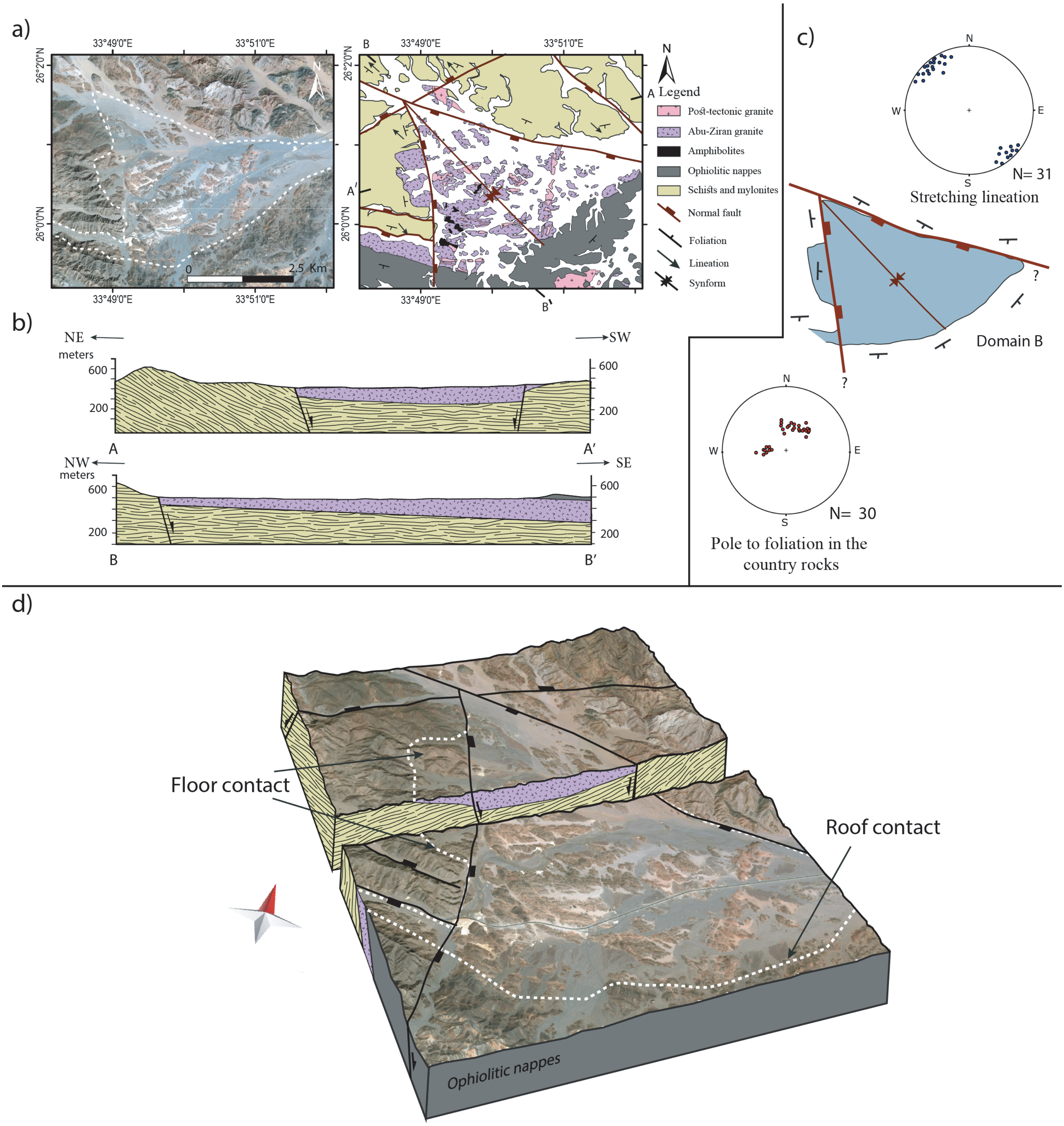

a)
33°49'0"E
33°51'0"E
26°2'0"N
26°0'0"N
0
2.5 Km
B
A
A'
B'
N
Legend
Post-tectonic granite
Abu-Ziran granite
Amphibolites
Ophiolitic nappes
Schists and mylonites
Normal fault
Foliation
Lineation
Synform
b)
NE
SW
meters
600
200
A
A'
NW
SE
B
B'
c)
N
W
E
S
N= 31
Stretching lineation
Domain B
?
N= 30
Pole to foliation in the country rocks
d)
Floor contact
Roof contact
Ophiolitic nappes

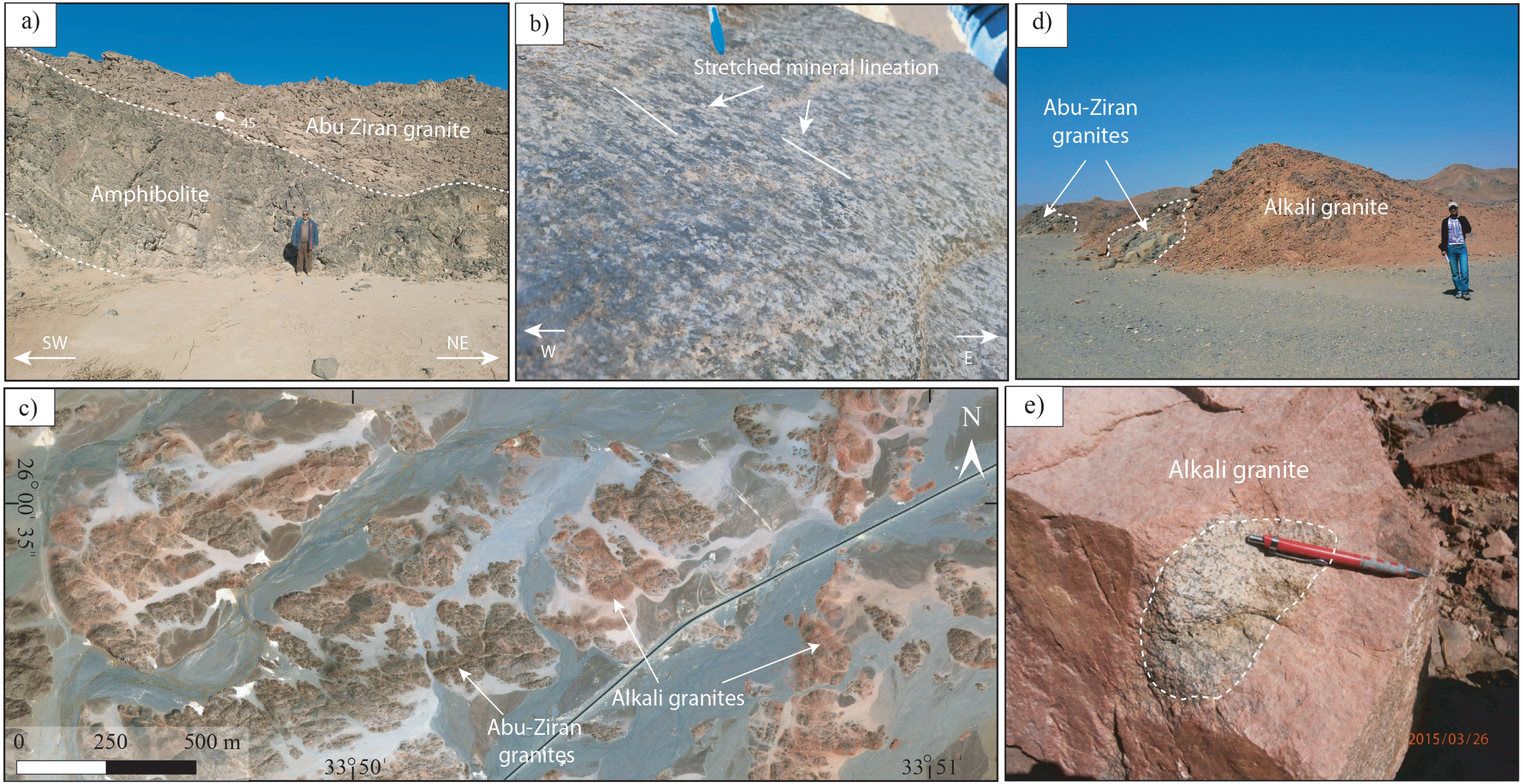
a)
Abu Ziran granite
45
Amphibolite
SW
NE
b)
Stretched mineral lineation
W
E
d)
Abu-Ziran
granites
Alkali granite
c)
N
26° 00' 35"
Alkali granites
Abu-Ziran
granites
0
250
500 m
33° 50'
33° 51'
e)
Alkali granite
2015/03/26

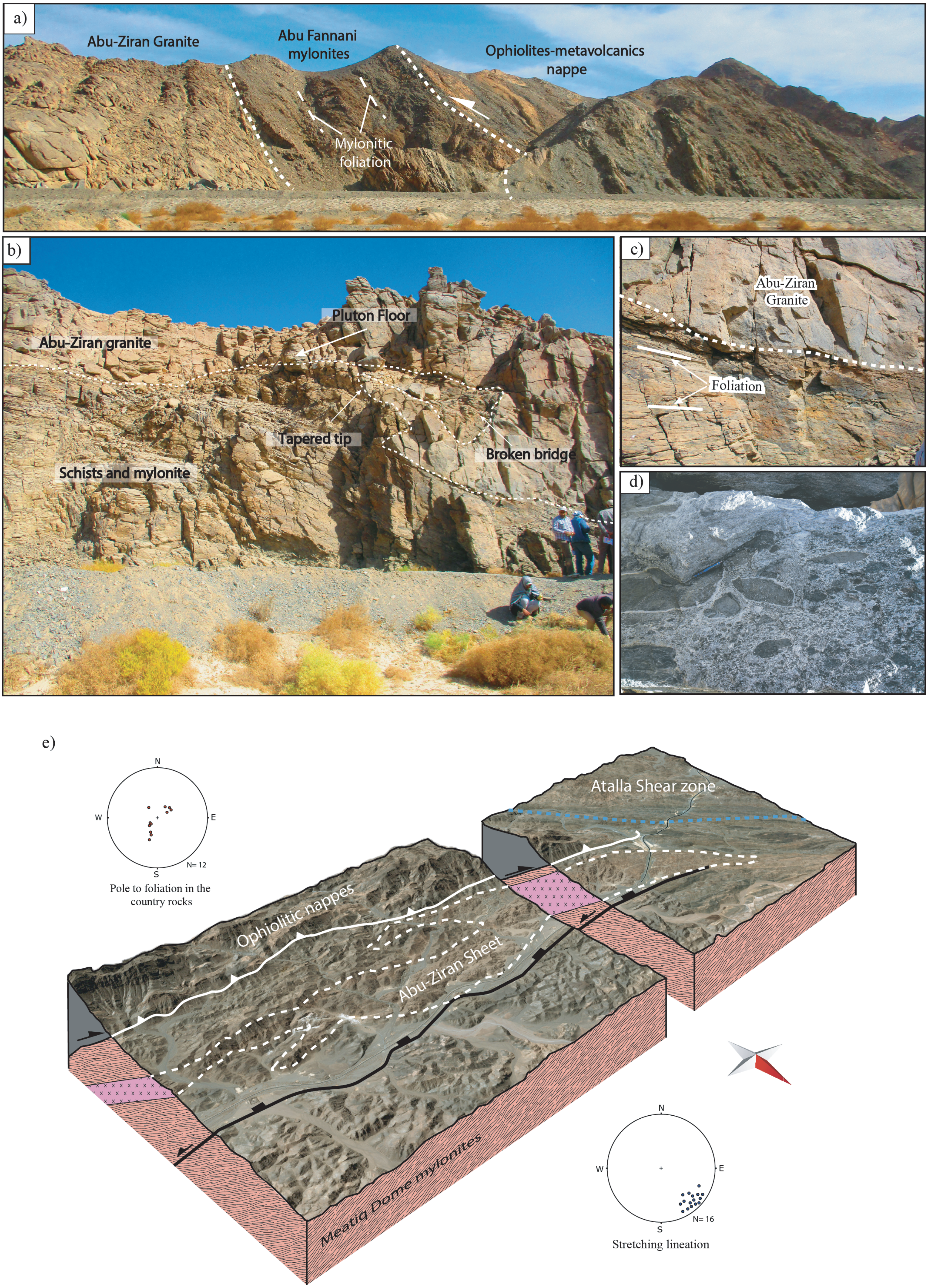
a)
Abu-Ziran Granite
Abu Fannani
mylonites
Ophiolites-metavolcanics
nappe
Mylonitic
foliation
b)
Pluton Floor
Abu-Ziran granite
Tapered tip
Broken bridge
Schists and mylonite
c)
Abu-Ziran
Granite
Foliation
d)
e)
N
W
E
S
N= 12
Pole to foliation in the
country rocks
Atalla Shear zone
Ophiolitic nappes
Abu-Ziran Sheet
Meatiq Dome mylonites
N
W
E
S
N= 16
Stretching lineation

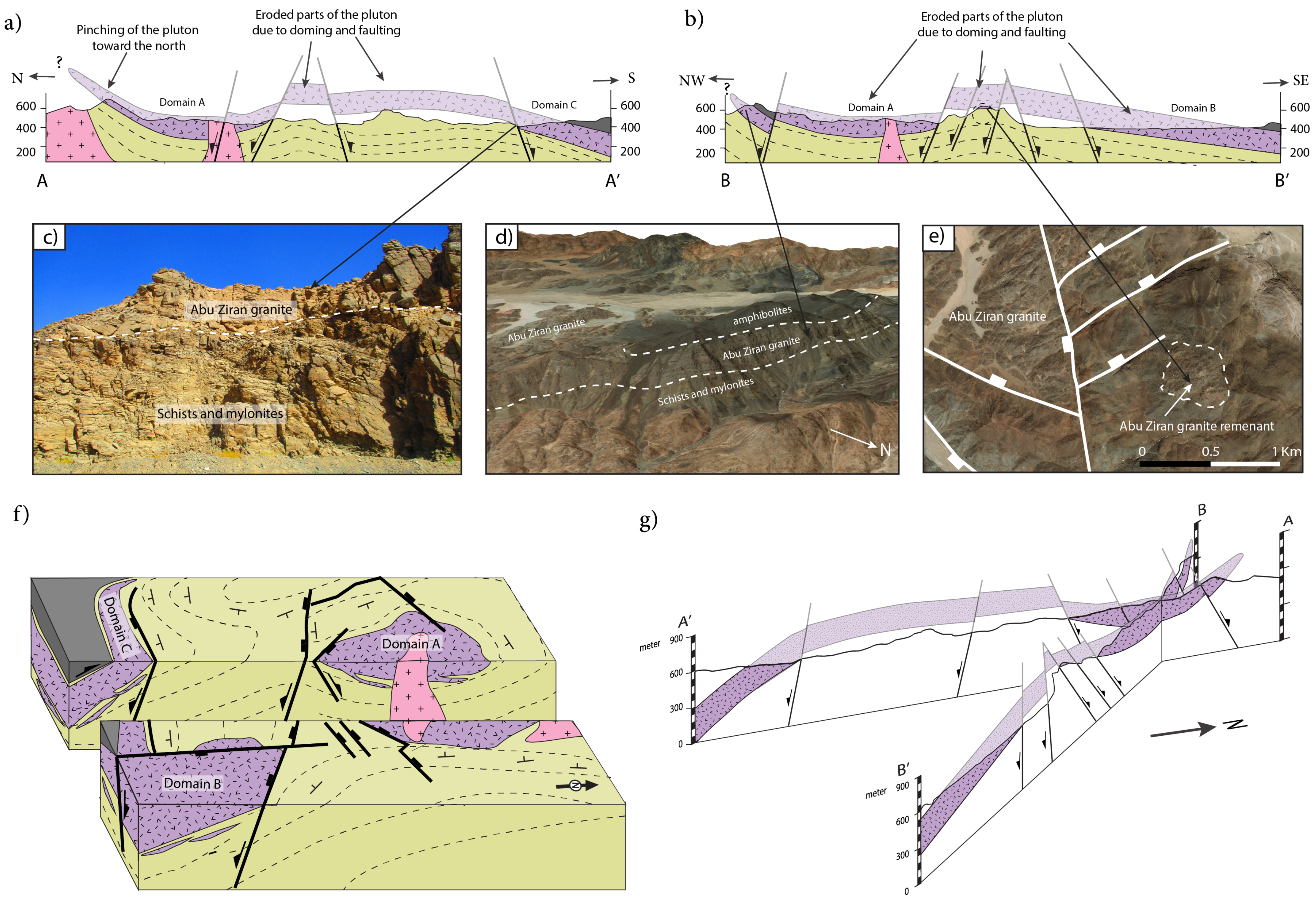

a)
Pinching of the pluton toward the north
Eroded parts of the pluton due to doming and faulting
N
S
Domain A
Domain C
600
400
200
A
A′
b)
Eroded parts of the pluton due to doming and faulting
NW
SE
Domain A
Domain B
B
B′
c)
Abu Ziran granite
Schists and mylonites
d)
Abu Ziran granite
amphibolites
Abu Ziran granite
Schists and mylonites
N
e)
Abu Ziran granite
Abu Ziran granite remenant
0
0.5
1 Km
f)
Domain C
Domain A
Domain B
g)
B
A
A′
meter
900
600
300
0
B′

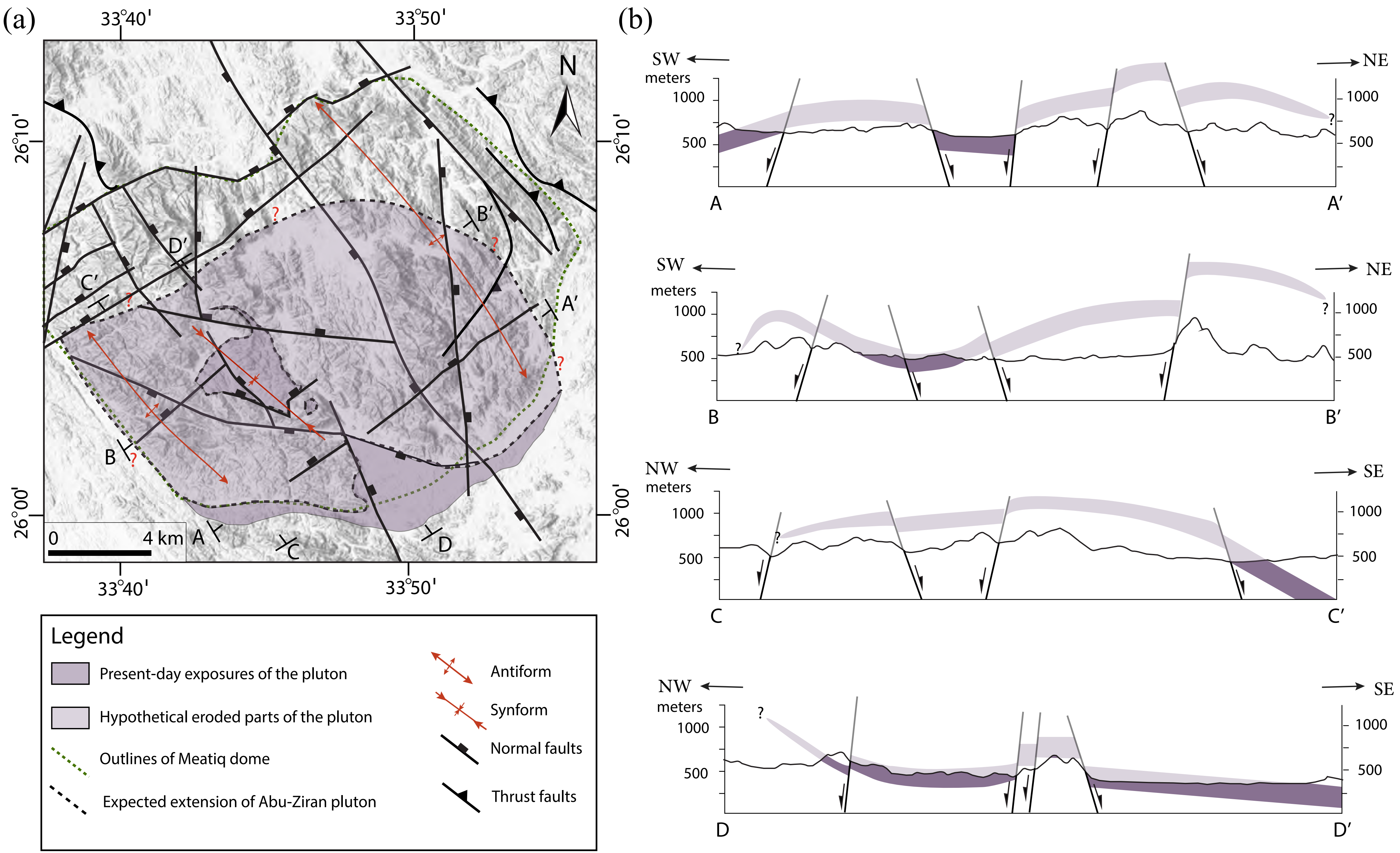

(a)
33°40'
33°50'
26°10'
26°00'
0
4 km
A
A′
B
B′
C
C′
D
D′
N
Legend
Present-day exposures of the pluton
Hypothetical eroded parts of the pluton
Outlines of Meatiq dome
Expected extension of Abu-Ziran pluton
Antiform
Synform
Normal faults
Thrust faults
(b)
SW
NE
NW
SE
meters
1000
500

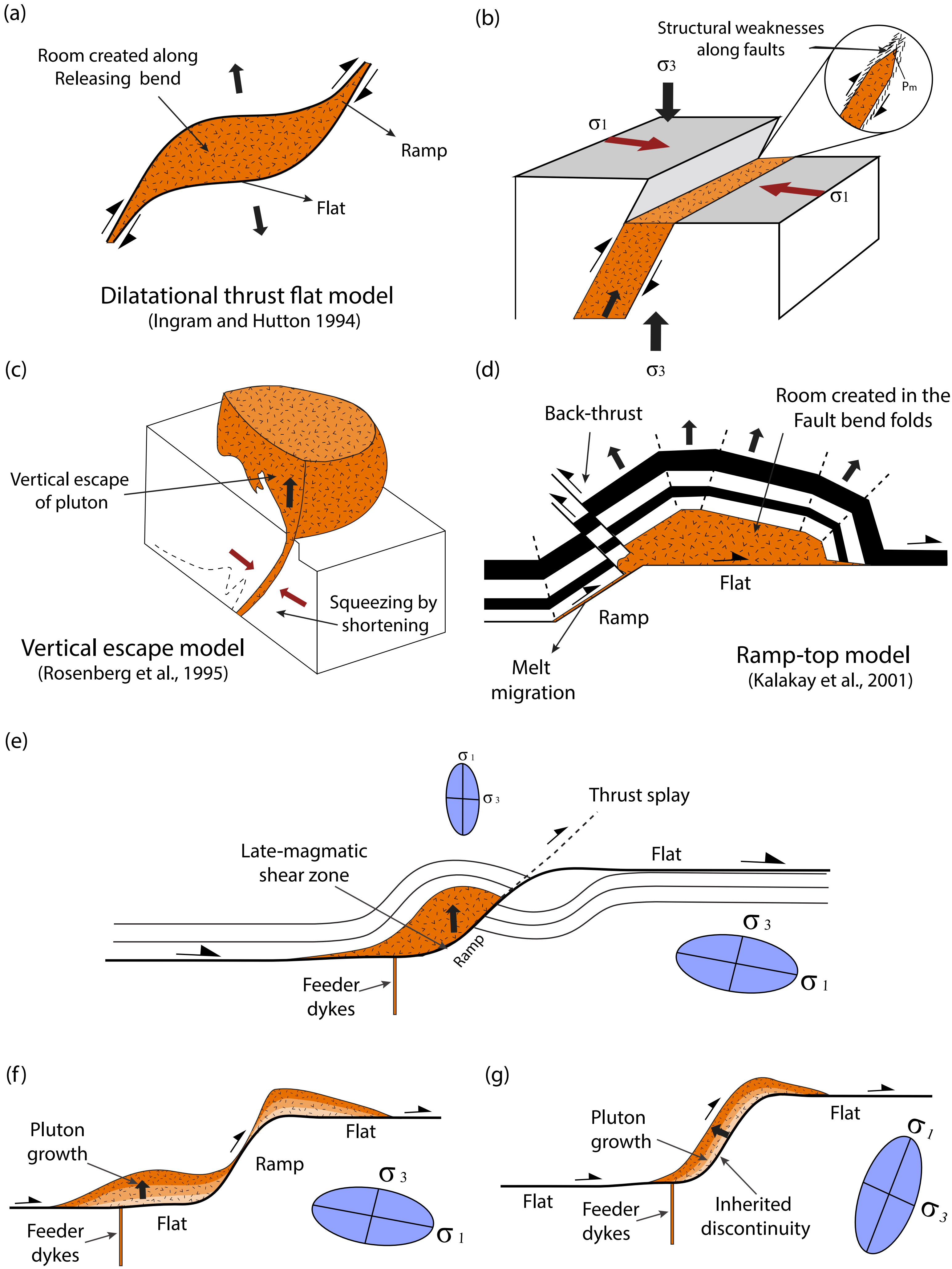

(a)
Room created along
Releasing bend
Ramp
Flat
Dilatational thrust flat model
(Ingram and Hutton 1994)
(b)
Structural weaknesses
along faults
σ3
σ1
Pm
σ1
σ3
(c)
Vertical escape
of pluton
Squeezing by
shortening
Vertical escape model
(Rosenberg et al., 1995)
(d)
Back-thrust
Room created in the
Fault bend folds
Flat
Ramp
Melt
migration
Ramp-top model
(Kalakay et al., 2001)
(e)
σ 1
σ 3
Thrust splay
Late-magmatic
shear zone
Flat
Ramp
σ 3
σ 1
Feeder
dykes
(f)
Pluton
growth
Flat
Ramp
σ 3
σ 1
Feeder
dykes
Flat
(g)
Pluton
growth
Flat
σ 1
Flat
Feeder
dykes
Inherited
discontinuity
σ 3

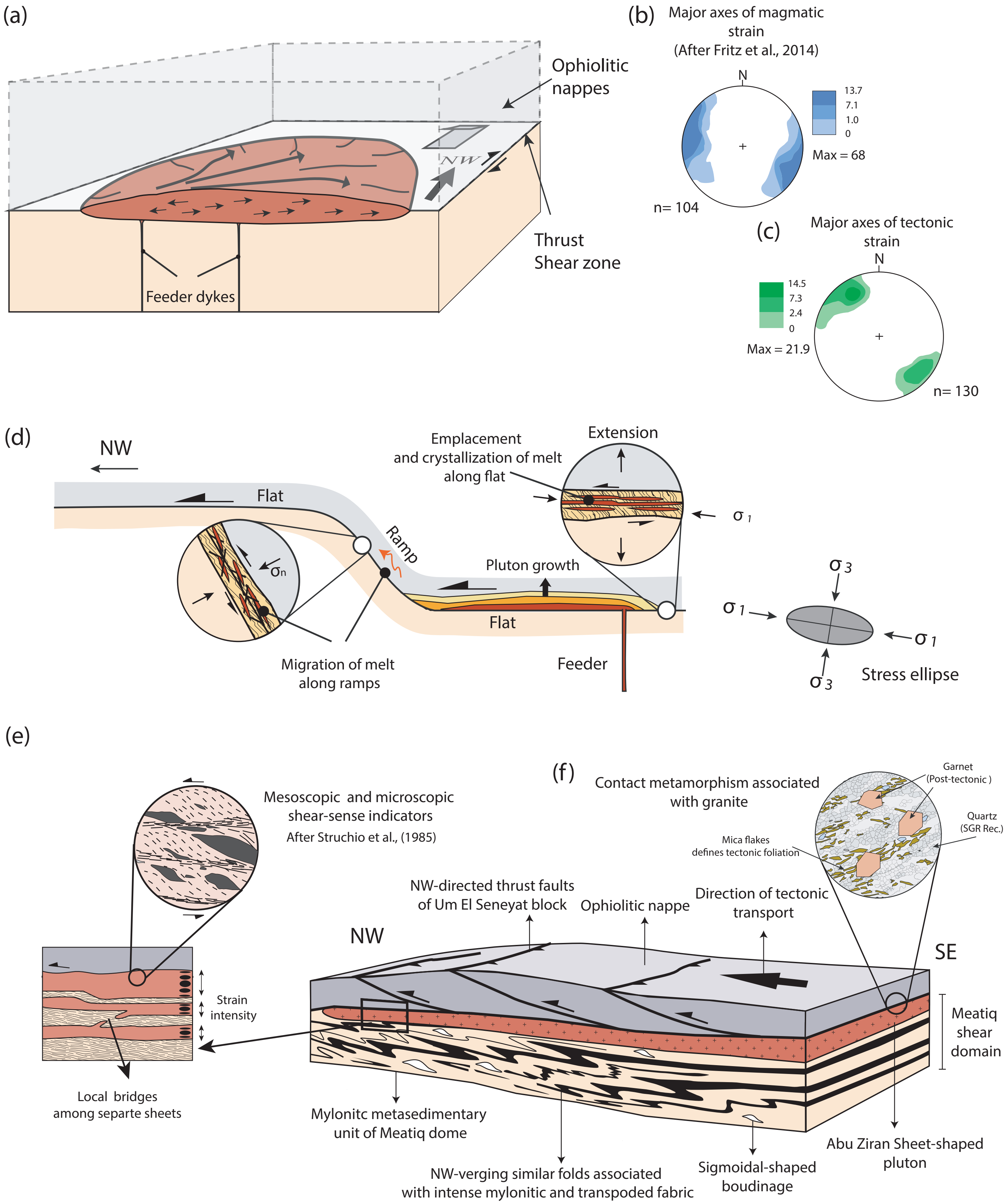

(a)
Ophiolitic nappes
NW
Thrust Shear zone
Feeder dykes
(b) Major axes of magmatic strain
(After Fritz et al., 2014)
N
13.7
7.1
1.0
0
Max = 68
n= 104
(c) Major axes of tectonic strain
N
14.5
7.3
2.4
0
Max = 21.9
n= 130
(d)
NW
Flat
Emplacement and crystallization of melt along flat
Extension
σ 1
Ramp
σn
Pluton growth
σ 3
σ 1
σ 1
σ 3
Flat
Migration of melt along ramps
Feeder
Stress ellipse
(e)
Mesoscopic and microscopic shear-sense indicators
After Struchio et al., (1985)
Strain intensity
Local bridges among separte sheets
(f) Contact metamorphism associated with granite
Garnet (Post-tectonic)
Quartz (SGR Rec.)
Mica flakes defines tectonic foliation
NW-directed thrust faults of Um El Seneyat block
Ophiolitic nappe
Direction of tectonic transport
NW
SE
Meatiq shear domain
Mylonitc metasedimentary unit of Meatiq dome
NW-verging similar folds associated with intense mylonitic and transpoded fabric
Sigmoidal-shaped boudinage
Abu Ziran Sheet-shaped pluton